Insurance Institute for Business & Home Safety

Where building science leads to real-world solutions.

Wind Loads on Small Roof-Mounted Air-Conditioning Units

Murray J. Morrison, PhD

Research Engineer

Insurance Institute for Business & Home Safety

June 5, 2013

IBHS – RC01 – 2013

Table of Contents

List of Figures

List of Tables

Abbreviations and Symbols

A: Projected area of the roof-mounted equipment perpendicular to the wind direction
CFx: Non-dimensional force coefficient in the x direction
CFy: Non-dimensional force coefficient in the y direction
CFz: Non-dimensional force coefficient in the z direction
CMx: Non-dimensional moment coefficient for moment about the x axis
CMy: Non-dimensional moment coefficient for moment about the y axis
CMz: Non-dimensional moment coefficient for moment about the z axis
DOF: Degrees of freedom for the force balances i.e. *Fx, Fy, Fz, Mx, My, Mz*
ε_{CFx}, ε_{CFy}, ε_{Cfz}, ε_{CMx}, ε_{CMy}, ε_{CMz}: Error in force and moment coefficients
F: Factor to convert from coefficients based on mean wind speed to coefficients based on gust wind speed
Fx: Force in the x direction
Fy: Force in the y direction
Fz: Force in the z direction
GCr: Force coefficient for roof-mounted equipment from the ASCE7-10
h: Height of the bottom of the roof-mounted equipment above the roof surface
L: Vertical distance from the top surface of the force balance (roof surface) to the geometric center of the roof-mounted equipment for *CMx* and *CMy* and half the projected width of the unit perpendicular to the wind direction for *CMz*
M: Force balance calibration matrix
Mx: Moment about the x axis
My: Moment about the y axis
Mz: Moment about the z axis
N: Number of calibration points for each force balance
PS_u: Power spectrum of the longitudinal velocity component
RME: Roof-mounted equipment
V: Mean wind velocity at building roof height (900 second average)

Abstract

This investigation examines wind loads on numerous configurations of roof-mounted equipment (RME). The testing examined the effects of unit porosity, location on the roof and elevation above the roof on wind loads for RME. Custom-designed force balances were used to measure wind forces and moments in six degrees of freedom. Overall, force coefficients for RME in ASCE7-10 were found to envelope the force coefficients for all configurations tested in the study with the exception of gooseneck vents and units elevated significantly above the roof surface. In general, the wind loads on RME are unaffected by unit porosity; however, the results suggest that modeling RME as a solid unit (no venting) leads to an overestimation of the forces in the vertical (z) direction. Since model scale wind tunnels typically use non-porous models, the results suggest that the vertical force on RME may be overestimated in these facilities. Within the scope of the investigation, the location on the roof appeared to have little effect on the RME forces, while the forces tended to increase with increasing elevation above the roof surface. Finally, substantial reductions in the wind forces on RME due to shielding effects from upwind units are observed. While the effects of shielding from clusters of upwind units does not justify reducing design loads on a mass-produced unit, it is an indicator of the possible benefits of screens and obstructions in reducing loads, if they surround and shield the unit or cluster of units.

1 Introduction

Failure of roof-mounted equipment (RME) during high-wind events can cause significant damage to the building where the RME is mounted as well as other buildings down wind. The failure of these elements can lead to tearing of the roofing membrane, which may result in a partial or total loss of the roof cover system. Ensuing water intrusion can cause substantial damage to the building and its contents. Sensitive electronic equipment, manufacturing equipment and other types of building contents frequently require a lead time for replacement, and building material shortages are common following a major hurricane. Building material availability and equipment replacement delays can prevent a business owner from returning to a normal level of service following a wind event. The combination of property damage and business interruption not only results in a significant increase in insured losses, but also may affect the insured's market share and the ability of the business to stay open following a disaster. Significant damage to roof-mounted equipment was observed following Hurricane Katrina, as outlined in FEMA 549 (2006).

The code wind load provisions for roof-mounted equipment in ASCE7-10 (2010) are primarily based on wind loads obtained from model scale wind tunnel measurements by Hosoya et al. (2001) and Kopp and Traczuk (2007). The study by Kopp and Traczuk (2007) provides the basis for the lateral and uplift wind force coefficients used in ASCE7-10 (2010). This study showed that the effects of wind flow over the roof, including shear layers and vortices, increase wind loads on RME. The effects were found to be greatest near the edges of the roof. However, increased loads extend a significant distance away from the edges and corners of the roof.

More recently, a study by Erwin et al. (2011) examined the wind loads on full-scale roof mounted air-conditioners using Florida International University's Wall of Wind facility. The results of Erwin et al. have been used to suggest that wind loads on roof-mounted equipment in ASCE7-10 (2010) may be un-conservative by as much as 50 percent for lateral loads. However, that suggestion is based on the extrapolation of results from short duration (3-minute) tests to equivalent peak loads for a one hour event. The three minute wind record shown in the report had high-frequency wind fluctuations superimposed on a somewhat sinusoidal wind record. Consequently, extrapolation using typical variations in natural winds may lead to significant overestimation of expected peak force coefficients. A direct calculation of the lateral force coefficient based on the peak lateral loads and the corresponding peak wind velocity during the published three-minute record results in lateral coefficients that are in general agreement with the ASCE7-10 (2010) lateral force coefficient. Blockage effects and the size of the equipment relative to the size of building used in the study may have also contributed to a distortion of results in this Florida International University study (Erwin et al., 2011). However, these experiments did indicate that screens could be effective in reducing the loads on the equipment by 33 percent to 70 percent.

Full-scale experiments allow the complex physical details of roof-mounted equipment to be correctly represented in the experiments. These details include complex flow features, such as air flow through the small openings in porous air conditioning units or screen walls as well as, flow underneath elevated air conditioning units. These details are more difficult to simulate correctly at model scale due to both the model's size and Reynolds number effects. The primary challenge for experiments conducted in full scale wind tunnel facilities is the correct simulation and match of the atmospheric boundary layer wind characteristics that are important for reproducing the flow around the test building and the surface pressures. The Insurance Institute for Business and Home Safety (IBHS) has demonstrated its ability to correctly simulate full-scale wind characteristics and surface pressures on low-rise buildings at a scale of 1:1 (Morrison et al., 2012).

This report presents results of an investigation that determined wind loads on RME units on a flat roof low-rise building. Tests were conducted in the IBHS Research Center's large wind tunnel using full-scale RME mounted on the roof of a full-scale building. The primary objective of the investigation was to determine whether ASCE7-10 (2010) RME wind load provisions adequately envelope the wind loads experienced by RME without being overly conservative.. This was accomplished by conducting measurements of RME wind loads using actual full-scale units installed on a full-scale building to examine the effects of unit venting styles (varying porosity), elevation above the roof, location on the roof, and grouping of units (shielding). Test configurations concentrated on locations of units near the upwind edges of the building roof where loads are expected to be highest. Results are compared to the code wind loads for RME provided by ASCE7-10 (2010).

2 Experimental Setup

The loads on full-scale RME were measured for installations on a full scale, flat roof low rise building in the IBHS Research Center's wind tunnel. This wind tunnel uses 105 vane axial fans installed in 15 cells arranged in five towers with three rows of cells in each tower. Cells in the bottom row contain nine fans housed in arrays, which are in three cells wide by three cells tall. The middle and upper rows of cells contain six fans per cell in arrays that are three wide by two tall. Precast panels that form the horizontal boundaries between the lower/middle and middle/upper cells are located at 4.27 m and 6.71 m. General details of the IBHS large wind tunnel can be found in Liu et al. (2011) and Morrison et al. (2012). Specific details regarding the experiment setup, instrumentation, and test plan are provided in this section.

2.1 Flow Field

The flow field in the IBHS test chamber has undergone a detailed development and validation process. Throughout this process, adjustments were made to improve the match between the simulated flow and full-scale atmospheric boundary layer (ABL) flow characteristics. The most notable adjustment was the addition of spires to the lower and middle fan cells, which proved to be critical in accurately duplicating the surface pressures on a building (Morrison et al., 2011). Figure 1 presents the vertical profiles of mean velocity and turbulence intensity of the longitudinal velocity component for the flow simulation used in this study compared to theoretical profiles obtained from ESDU (1982) and to field observations obtained from the Wind Engineering Research Field Laboratory at Texas Tech University (Smith, 2010). The overall comparison between the IBHS results and the benchmark profiles is good. The solid heavy horizontal lines in Figure 1 identify the heights of the cell boundaries discussed above. Effects of the cell boundary can be observed in the mean velocity profile (left) but not in the turbulence profile (right). The longitudinal turbulence spectra, shown in Figure 2, shows generally good agreement with field and theoretical power spectra. However, a spectral gap (decrease in spectral content) exists between wave numbers of 0.01 and 0.1 in the IBHS flow field as compared to both the field observation and theoretical profiles. Complete details of the flow simulation used in the investigation are presented in Morrison et al. (2012). Despite this spectral gap, Morrison et al. (2012) have shown that the surface pressures on a building in the IBHS test chamber match reasonably well with both field observations and model scale wind tunnel results. For this investigation, the mean (15 minute average) wind speed at roof height is approximately 17 m/s (38 mph) for all experiments.

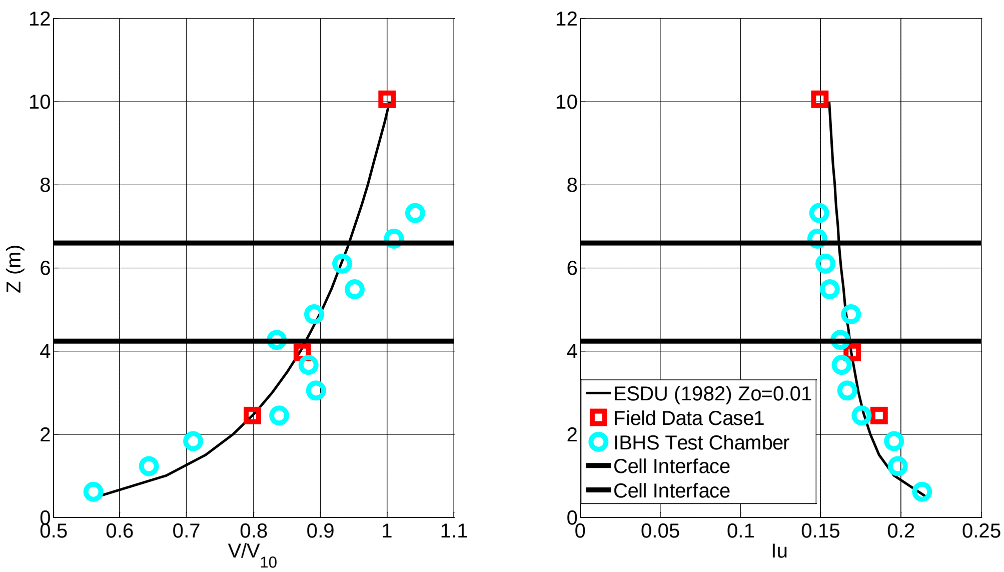

Figure 1: Variation of mean velocity (left) and turbulence intensity of longitudinal velocity component (*Iu*) (right) with height

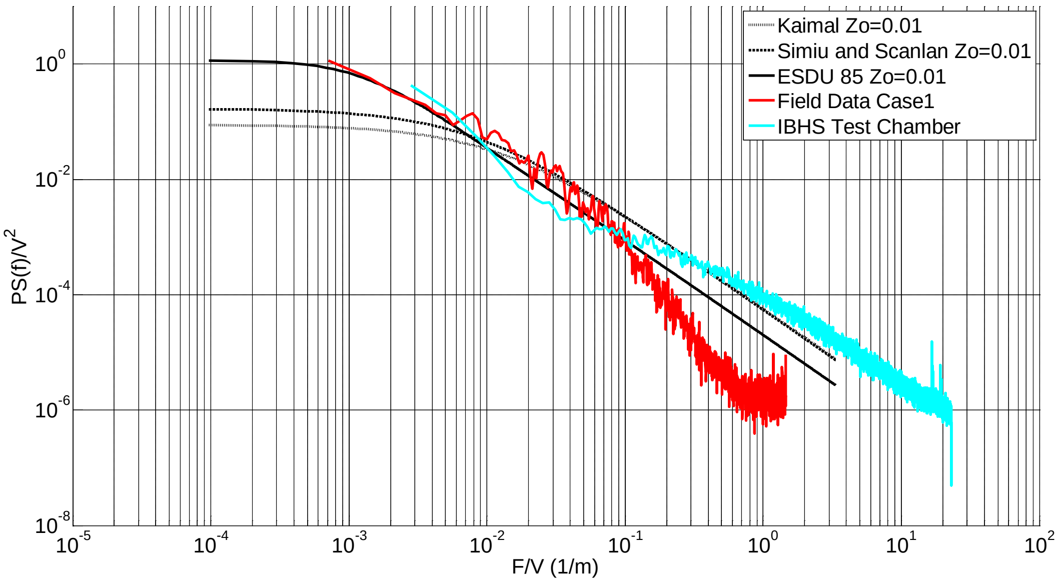

Figure 2: Power spectrum of longitudinal velocity component (PS_U)

2.2 Building Details

A flat-roofed building with plan dimensions 9.14 m (30) by 12.2 m (40 ft.) and an eaves height of 3.96 m (13 ft.) was used for all RME configurations in the present study. Figure 3 shows the test building during various stages of construction. The building consisted of an internal steel frame and metal roof deck as shown in Figure 3 A and B. A false wooden roof was constructed above the steel roof deck and consisted of 20, 1.5 m (5 ft.) by 1.2 m (4 ft.) removable wooden sections, which are shown standing on edge in Figure 3 C. Each of these wooden sections could be removed individually to allow a force balance (discussed in greater detail in section 2.4.1) to be installed at that location on top of the steel deck while maintaining a flat roof surface. The walls of the building were also constructed from modular wooden wall sections. Figure 3 D shows the completed test building with a piece of equipment installed on top of a force balance on the roof. The building was located at the center of the turntable in the IBHS wind tunnel with the windward wall nominally 8.7 m (28.5 ft.) downstream of the wind vanes. Figure 4 shows the locations and naming convention of the possible force balance locations.

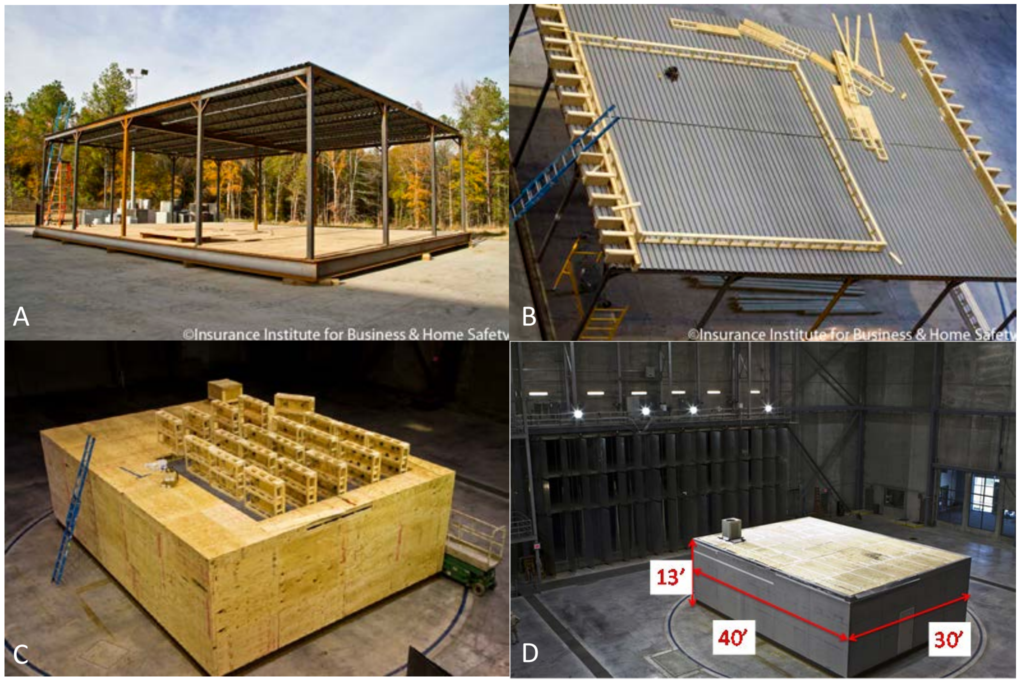

Figure 3: RME test building during different stages of construction

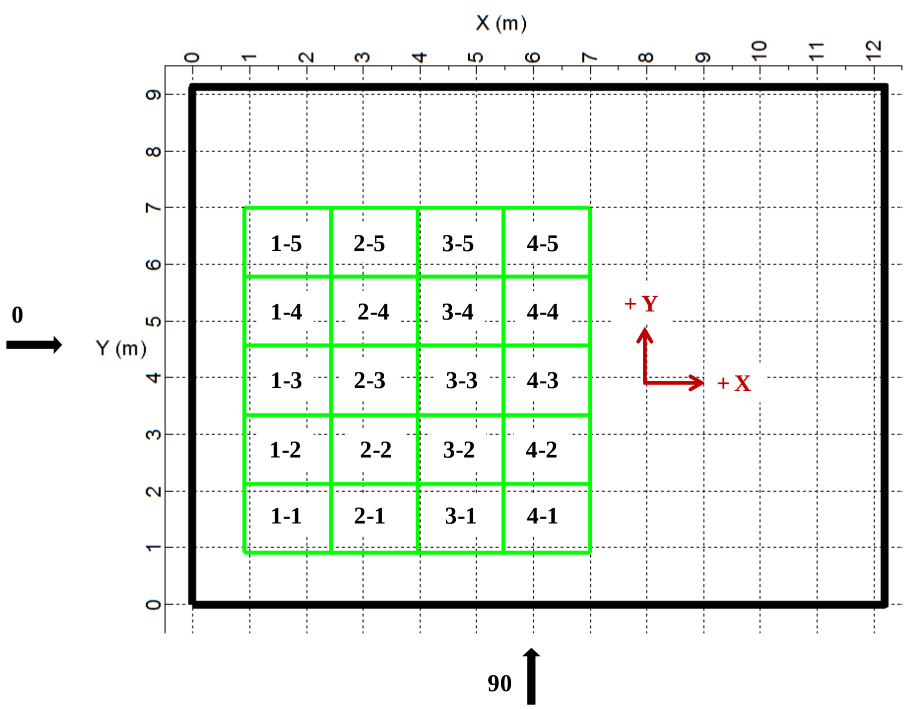

Figure 4: Layout of possible force balance locations on the roof of the building and naming convention

2.3 Roof-Mounted Equipment Inventory

The RME used in the investigation were primarily decommissioned condenser air conditioning units. Figure 5 shows the overall collection of RME obtained by IBHS. In total, IBHS obtained 19 small air-conditioning units, three larger roof top package units and two circular roof vents. In addition, IBHS purchased two goosenecks vents (not shown in Figure 5), one with a rectangular cross section and one with a round cross section. Not all the equipment obtained by IBHS was used in the investigation. Specific dimension details of the tested units are provided in section 3.

Figure 5: Overview of all the RME units obtained by IBHS

2.4 Instrumentation

The experiment used force balances to measure the reaction forces on RME. The following section outlines the experimental setup of the force balances used in the study. For all experiments the data was collected at a rate of 200 Hz for duration of 900s. For each experimental configuration, seven different wind angles were tested ranging from 0° to 90° (as defined in Figure 4) in 15° increments.

2.4.1 Force Balances

Custom force balances shown in Figure 6 , were designed and built by IBHS to measure the wind loads on RME. The force balance consists of a 25.4 mm (1 in.) aluminum base plate and an aluminum frame supported by seven loads cells arranged as indicated in Figure 6 (right). Both the base plate and support frame are designed to have a high stiffness, so that the support condition does not affect the measured loads. Protective aluminum sides and cover are used to encase the support frame and load cells but are not part of the force measurement system. The loads are transferred to the support frame via four mounting points shown in Figure 6 (left). Sufficient clearance exists around the mounting points to prevent load transfer to the aluminum cover. A total of three force balances of this design were constructed for the measurements. In order to mount numerous RME of different shapes and sizes, a modular rail system was used to attach the equipment to the mounting points on the force balance. Figure 7 shows a piece of RME attached to a force balance using this modular rail system. For a majority of the RME used in the study there were no clear attachment points integral to the RME, which could be used to secure the equipment to the rail system. The study used steel strapping which was screwed into the casing of the equipment and then attached the rail system to provide the required attachment. This method of attachment did not influence the measured forces, which is the objective of the study.

Due to the height of the rail system, the lowest mounting elevation for RME on a force balance was 0.14 m (5.5 in.) above the roof deck.

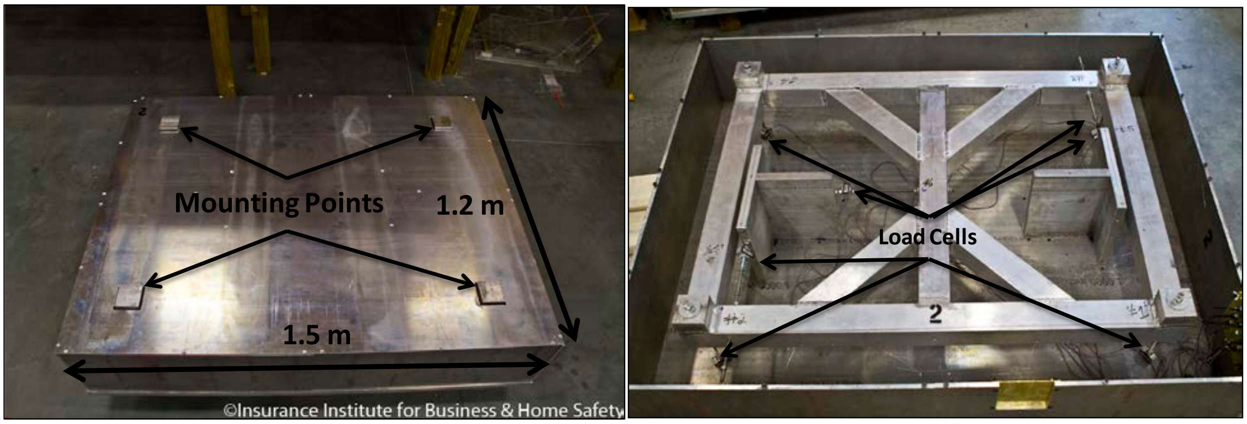

Figure 6: Overview of custom force balances constructed by IBHS

Figure 8 presents the coordinate system for the forces and moments on a single force balance. The force balances were always oriented the same way when installed on the roof of the building so that the orientation of the force balance coordinate system and the coordinate system shown in Figure 4 are the same. Four 2230 N (500 lbs) load cells are oriented to measure the force in the '*z*' direction, one 892 N (200 lbs) load cell measures the force in the 'x' direction and two 892 N (200 lbs) load cells measure the force in the 'y' direction. APPENDIX A provides a list and location of the loads cells in each of the force balances. The arrangement of the loads cells allow the force balance to resolve three orthogonal forces and three orthogonal moments, for a total of 6 degrees of freedom (DOF) as indicated in Figure 8. The capacity of the force balance for each DOF is shown in Table 1.

Figure 7: RME attached to a force balance using the modular rail system

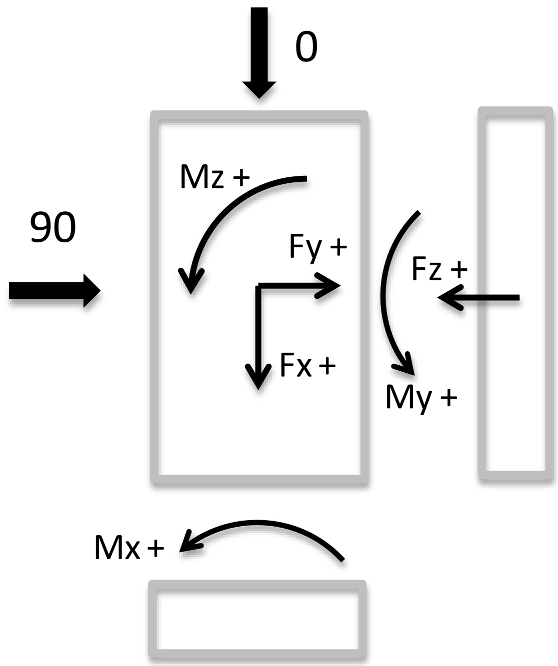

Figure 8: Coordinate system for forces and moments

Table 1: Capacities of the force balances for each degree of freedom (DOF)

DOF	*Fx*	*Fy*	*Fz*	*Mx*	*My*	*Mz*
Capacity	892 N (200 lbs)	1784 N (400 lbs)	8918N (2000 lbs)	3737 Nm (2750 lbs- ft.)	5101 Nm (3753 lbs- ft.)	884 Nm (650 lbs- ft.)

2.4.2 Force Balance Calibration

To convert the individual readings obtained from each of the seven load cells (LC1, LC2,…LC7) to the three forces and three moments, the matrix *M* in Eq. (1) was determined through a calibration of each force balance. The *M* matrix also acts as a correction for any changes in the calibration constants since the factory calibration of the load cells. Figure 9 shows the force balance calibration apparatus used to experimentally determine the matrix *M*, for all three force balances. The test rig consists of a reaction frame which rests on the aluminum covers and a pulley system connecting a mounting post to a hangar where weight can be added. In line with the pulley is a load cell to measure the load applied to the mounting post. This approach provides a direct measurement of the force applied to the balance and omits any friction losses of the pulley. The mounting post can be positioned anywhere within the x-y plane of the force balance and the pulley can be attached to the mounting post at three different heights. This allows for forces and moments to be applied in all 6 DOF. Typically, a total of 108 individual calibration points were used to generate the calibration *M* matrix for each force balance. These 108 data points represent an over-defined system of equations for the 42 unknowns of matrix *M*. The optimal matrix *M* is then determined by the matrix division of Eq. (1), shown in Eq. (2), where *N* represents the number of calibration points. APPENDIX B presents the calibration matrix, *M*, determined for each of the force balances used in the investigation. The errors associated with the best fit of the calibration matrix *M* as a percentage of full scale range are also presented in APPENDIX B.

$$[LC1 \quad LC2 \quad LC3 \quad LC4 \quad LC5 \quad LC6 \quad LC7]\begin{bmatrix} M_{11} & M_{12} & \dots & \dots & \dots & M_{16} \\ M_{21} & & & & & \vdots \\ \vdots & & & & & \\ \vdots & & & & & \\ \vdots & & & & & \\ \vdots & & & & & \\ M_{71} & \dots & & & & M_{76} \end{bmatrix} = \begin{bmatrix} Fx \\ Fy \\ Fz \\ Mx \\ My \\ Mz \end{bmatrix} \tag{1}$$

$$\begin{bmatrix} M_{11} & M_{12} & \dots & \dots & \dots & M_{16} \\ M_{21} & & & & & \vdots \\ \vdots & & & & & \\ \vdots & & & & & \\ \vdots & & & & & \\ \vdots & & & & & \\ M_{71} & \dots & & & & M_{76} \end{bmatrix} = \left[\begin{pmatrix} Fx \\ Fy \\ Fz \\ Mx \\ My \\ Mz \end{pmatrix}_1 \begin{pmatrix} Fx \\ Fy \\ Fz \\ Mx \\ My \\ Mz \end{pmatrix}_2 \dots \begin{pmatrix} Fx \\ Fy \\ Fz \\ Mx \\ My \\ Mz \end{pmatrix}_N \right] \backslash \begin{bmatrix} (LC1 & LC2 & LC3 & LC4 & LC5 & LC6 & LC7)_1 \\ (LC1 & LC2 & LC3 & LC4 & LC5 & LC6 & LC7)_2 \\ & & & \vdots & & & \\ (LC1 & LC2 & LC3 & LC4 & LC5 & LC6 & LC7)_N \end{bmatrix} \tag{2}$$

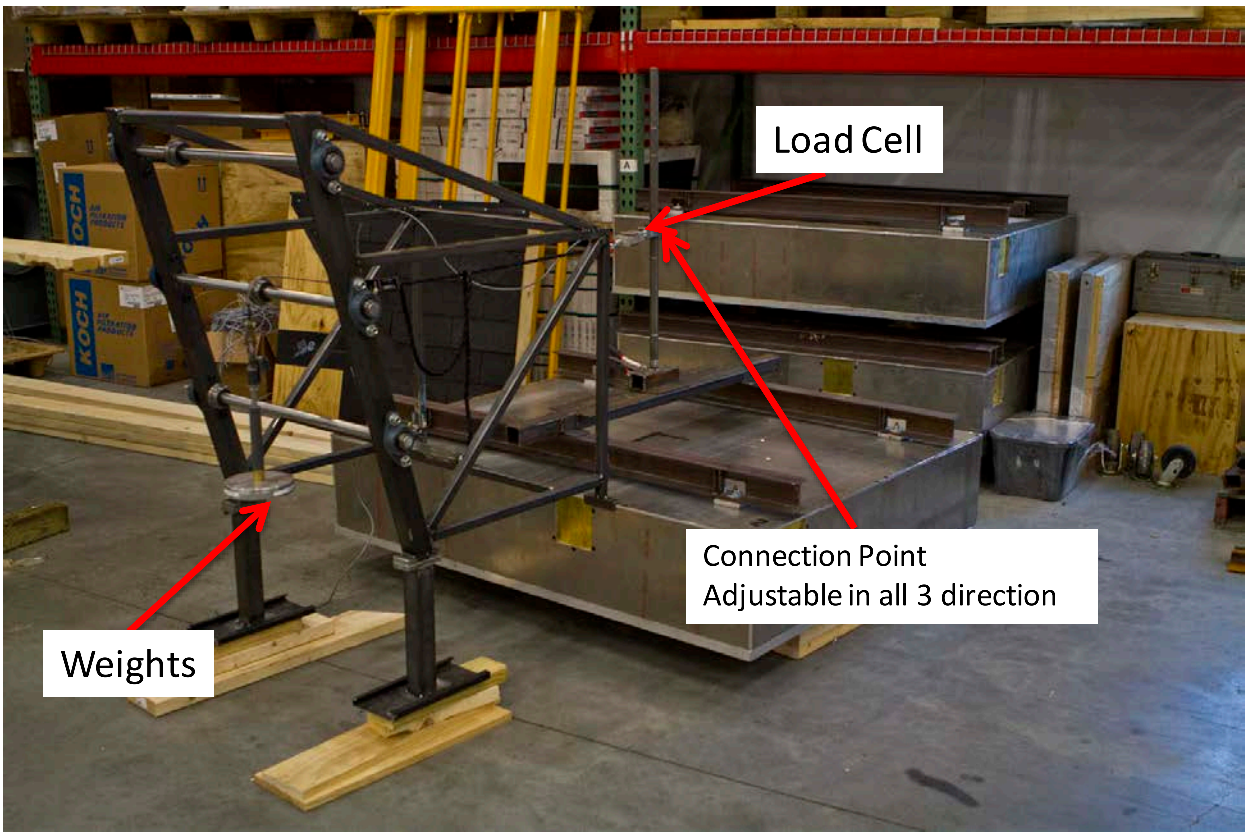

Figure 9: Force balance calibration setup

2.4.3 Wind Speed Measurement

Wind speed within the test chamber was monitored by a single RM Young anemometer in the middle cell of tower three (middle column of cells) similar to that described in Morrison et al. Validation measurements, when the building was not in the test chamber, have shown that the ratio of mean velocities between this RM Young anemometer and the roof height wind speed is 0.98. For the experimental program, the same simulated open country wind record was used to control the fans for all test configurations. This simulated wind record includes slightly different time histories for control of fans in different cells. The result is a wind field that reproduces typical lateral and vertical variations in instantaneous wind speeds as well as the variation in mean wind speed with height measured in atmospheric boundary layer winds. Monitoring of the RM Young anemometer is used to ensure that time average and peak wind speeds in the test chamber remained the same from test to test.

2.5 Data Reduction

The report presents all forces and moments obtained from the force balance as non-dimensional force coefficients that are directly comparable to the *GCr* coefficients provided in ASCE7-10 (2010) using:

$$CFx = \frac{Fx}{0.5\rho V^2 A} F \tag{3}$$

$$CFy = \frac{Fy}{0.5\rho V^2 A} F \tag{4}$$

$$CFz = \frac{Fz}{0.5\rho V^2 A} \mathrm{F} \tag{5}$$

$$CMx = \frac{Mx}{0.5\rho V^2 AL} \mathrm{F} \tag{6}$$

$$CMy = \frac{My}{0.5\rho V^2 AL} F \tag{7}$$

$$CMz = \frac{Mz}{0.5\rho V^2 AL} \mathrm{F} \tag{8}$$

where V is the 900s mean wind velocity at roof height of the building. Since ASCE7-10 (2010) uses three-second gust wind speeds and compatible pressure and force coefficients in its calculation of pressures, forces and moments, the factor, *F*, is used to convert the force and moment coefficients from values based on the 900s mean wind velocity to values based on maximum three-second gust wind speeds. The factor, *F*, was calculated using the method outlined by St. Pierre et al. (2005). For the experiments, *F* is computed to be 0.47. The area *A,* is the projected area of the unit perpendicular to the wind direction for *CFx, CFy, CMx, CMy* and the vertical projected area for *CFz* and *CMz*. The distance *L,* is the distance of the geometric center of the unit above the roof surface for *CMx, CMy* and is half the projected width of the unit perpendicular to the wind direction for *CMz*.

2.5.1 Point of Load Application

ASCE7-10 (2010) only specifies *GCr* coefficients that are to be used to calculate the lateral and uplift forces. Lateral forces are calculated based on the vertical projected area of the RME on a plane perpendicular to the direction of the wind. Vertical forces are calculated based on the horizontal cross-sectional area of the RME. The value of *GCr* for lateral forces is 1.9 while that for vertical forces is 1.5. *CFx* and *CFy* are directly equivalent to *GCr* for lateral forces and *CFz* is directly equivalent to *GCr* for vertical forces. No specific guidance is given on what elevation to use in applying the lateral force. The usual assumption would be to apply it at the centroid of the projected area. Since the normalizing length, *L*, used in the definition of the moment coefficients defined in equations 6 and 7 is the height of the centroid of the area of RME above roof level, equal values of lateral force coefficients and their corresponding moment coefficients would indicate that the lateral force should be applied at the centroid of the area. In addition, no guidance is given for calculating *CMz* from the *GCr* coefficients provided in ASCE7-10 (2010). As such, *CMz* for ASCE7-10 (2010) is not calculated for comparison purposes in the study.

2.5.2 Measurement Uncertainty

APPENDIX B presents the calibration matrix and errors associated with the calibration matrix for each DOF of all three force balances. The maximum fitting error for each force balance and DOF is presented in Table 2. The errors in the force coefficients defined in Eq. (3) through Eq. (8) will depend on the size of the unit and the height of the unit above the roof surface in the case of moment coefficients. While this error will be different for each unit, for the units tested the sixth column in Table 2 provides the worst error on each force or moment coefficient as a function of either *A* or *AL*. It should be noted that the errors presented in Table 2 assume that the only source of measurement error is due to the force balances. The only test results presented in this report using force balance three are in Figure 34. Consequently, for nearly all results presented in the report the force balance related errors in forces are less than 0.4 percent of the full scale range and the force balance related errors in moments are less than 0.8 percent of the full scale range.

Table 2: Maximum fitting error of the calibration matrices for each DOF per force balance as a percentage of full scale range

DOF	Force Balance #1	Force Balance #2	Force Balance #3	Error on Force Coefficients	
Fy	0.15	0.07	0.37	ε_{CFx}/A	0.012
Fx	0.36	0.32	1.26	ε_{CFy}/A	0.02
Fz	0.17	0.04	0.03	ε_{CFz}/AL	0.028
My	0.68	0.07	0.06	$\varepsilon_{CMx}/(AL)$	0.063
Mx	0.75	0.03	0.06	$\varepsilon_{CMy}/(AL)$	0.059
Mz	0.32	0.29	0.33	$\varepsilon_{CMz}/(AL)$	0.005

3 Results and Discussion

Results from this study represent only wind loads applied to the RME. The weight of the RME was subtracted from the measured forces prior to testing. The force coefficients presented follow the coordinate system defined in Figure 8.

3.1 Effect of Venting Styles

To examine the effect of venting style on the wind loads, two RME units with different venting styles were tested along with two representations of units with no venting. Units with no porosity, which are typical of RME used in model scale wind tunnels, are represented in this study by testing both a wooden box as well as a RME unit with its vents covered with sheet metal panels. Table 3 shows the four RME configurations tested and their corresponding dimensions. As shown in Table 3 the dimensions of each unit are nearly identical. The effects of venting were evaluated at 2 locations on the roof, location 1-1 and location 2-2, as shown in Figure 4. It should be noted that the case using ACU5 with covered vents was not tested at location 2-2.

Table 3: RME tested to examine effect of venting style

Name	Picture	Dimensions
Vent Style 1 (ACU7)		0.76 x 0.76 x 0.97 m 2.5 x 2.5 x 3.2
Vent Style 2 (ACU5 and ACU6)		0.83 x 0.72 x 1.03 m 2.7 x 2.4 x 3.4 ft.
Vent Style 2 with Covered Vents (ACU5)		0.83 x 0.72 x 1.03 m 2.7 x 2.4 x 3.4 ft.
Solid Box		0.76 x 0.76 x 0.97 m 2.5 x 2.5 x 3.2 ft.

Figure 10 through Figure 15 show the maximum, minimum and mean coefficients for each DOF versus wind angle for each of the venting styles shown in Table 3 at location 1-1. The variation of the wind loading coefficients for each DOF seems reasonable with the mean *CFy* and *CFx* being approximately zero at wind angles of 0° and 90° respectively. Figure 16 and Figure 17 present a summary of the maximum, minimum and mean force coefficients at the wind angle where the peak absolute coefficient occurs for each DOF, at locations 1-1 and 2-2 respectively. In general, the results from location 1-1 and 2-2 are very similar with perhaps slightly lower peak coefficients for each DOF at location 2-2. However, this small reduction is within the scatter of the data. For all DOF, the wind load coefficients in ASCE7-10

(2010) envelope the measured peak coefficients without being overly conservative. The study results show similar trends in values as a function of wind direction and a reasonable collapse of the data regardless of venting style with the exception of *CFz*. At both locations 1-1 and 2-2 the mean and peak *CFz* coefficients are significantly higher for the box and sealed vent cases than the cases were the vents were left open. This finding makes sense intuitively since for both venting styles the top of the units where the fan exhausts has a much higher net free area than the sides of the units. These results indicate that modeling RME as a solid box – which is typically done for model scale wind tunnel studies – provides reasonable lateral force coefficients for units with venting styles similar to those tested herein, but does tend to overestimate the uplift forces on the unit by approximately 40 percent.

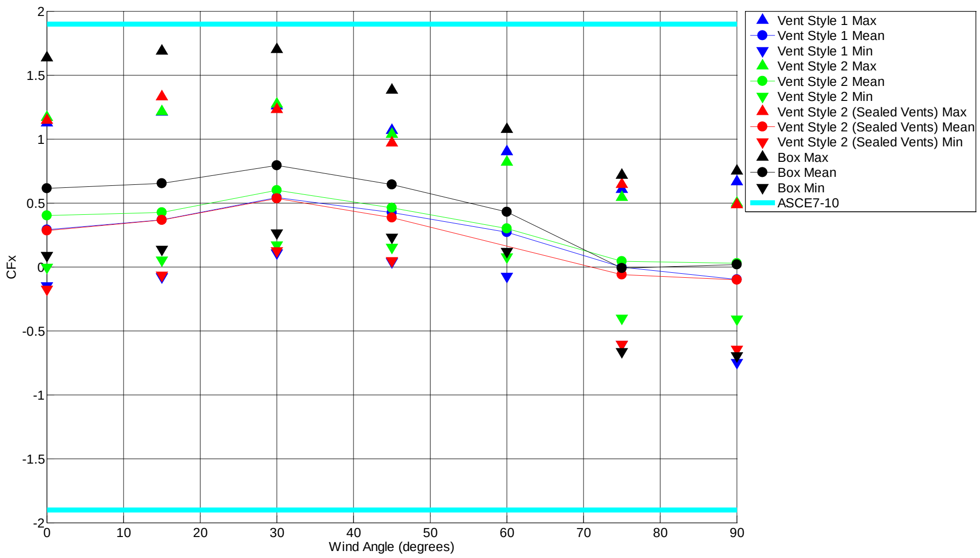

Figure 10: *CFx* along wind force coefficients for units with different venting style

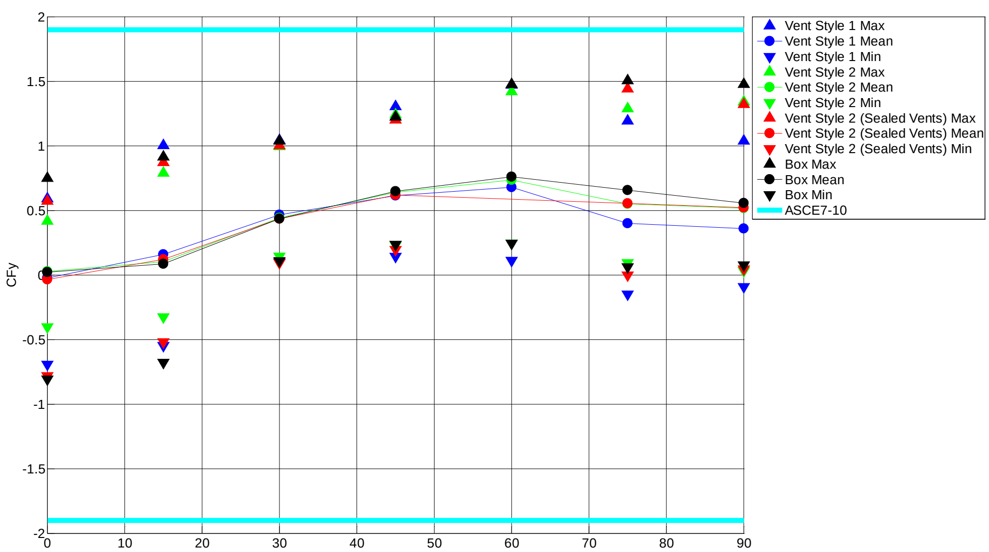

Figure 11: *CFy* lateral force coefficients for units with different venting style

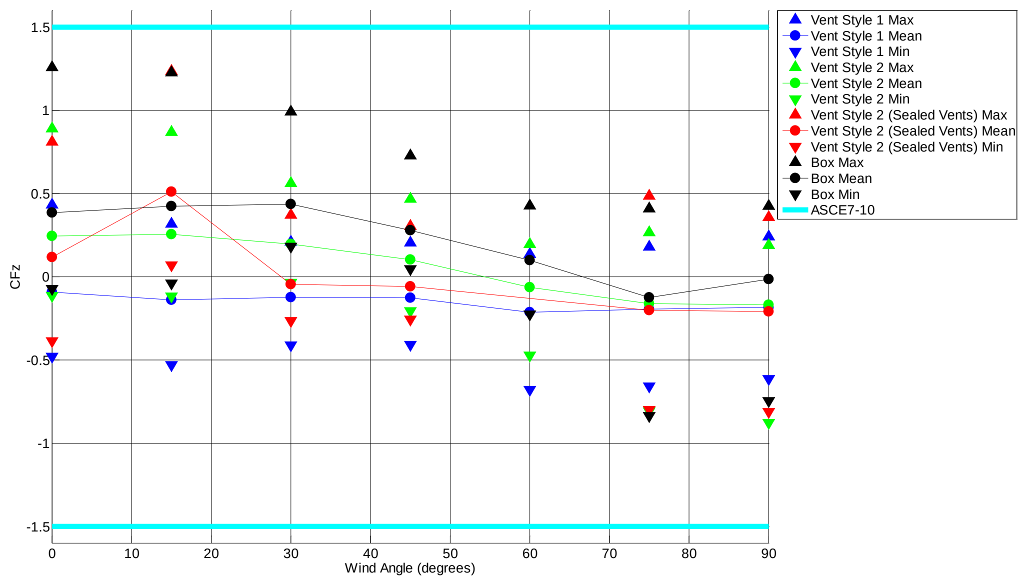

Figure 12: *CFz* uplift force coefficients for units with different venting style

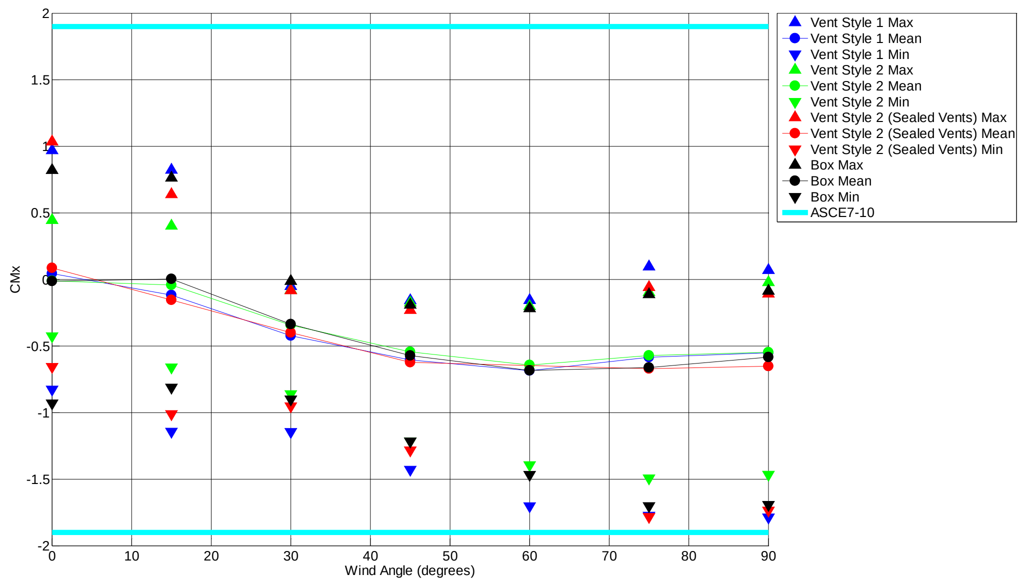

Figure 13: *CMx* moment coefficients for units with different venting style

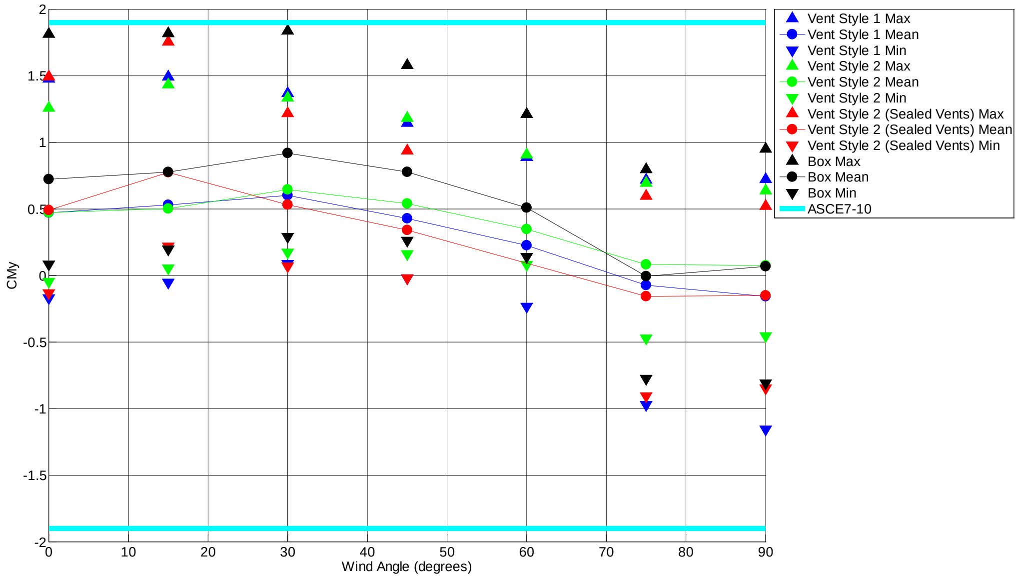

Figure 14: *CMy* moment coefficients for units with different venting style

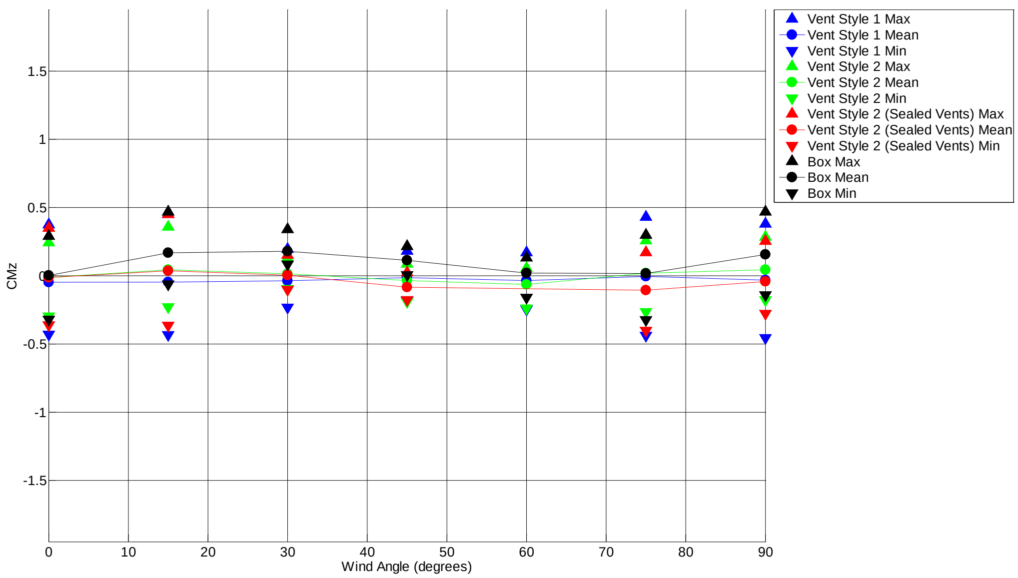

Figure 15: *CMz* moment coefficients for units with different venting style

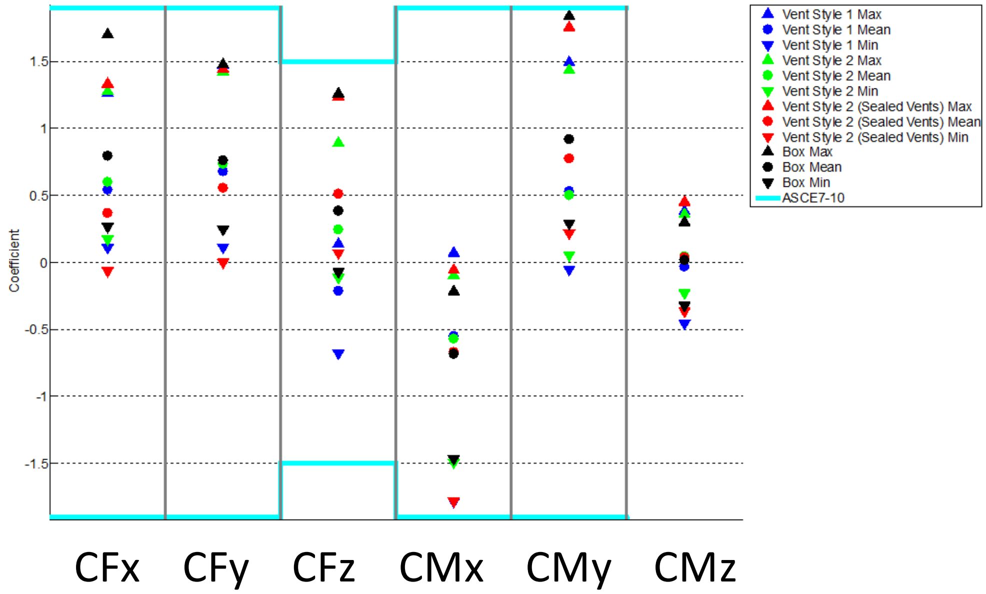

Figure 16: Summary of the max, min and mean coefficients for each degree of freedom for the wind direction that produces the highest loading coefficient at location 1-1

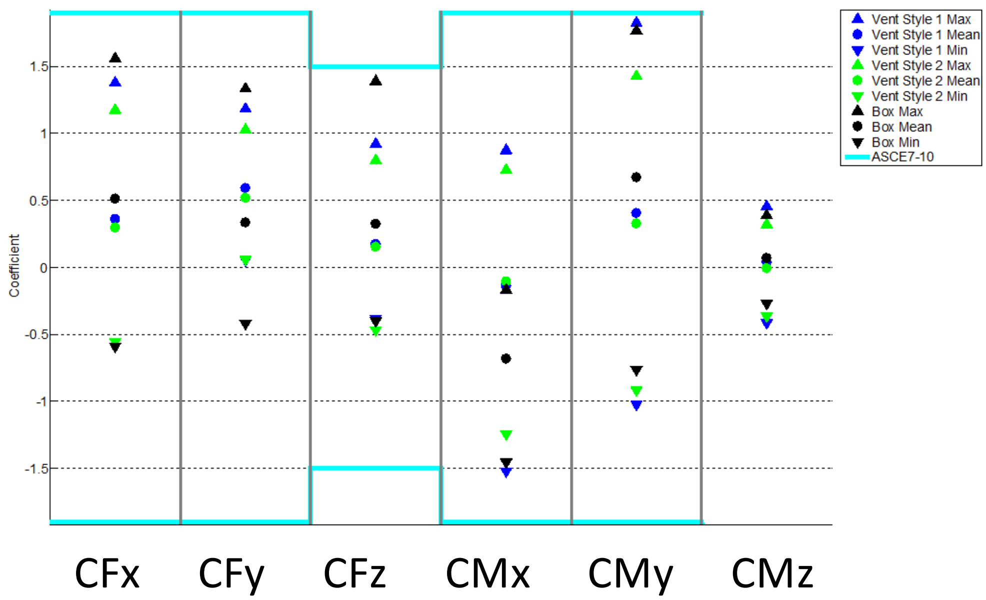

Figure 17: Summary of the max, min and mean coefficients for each degree of freedom for the wind direction that produces the highest loading coefficient at location 2-2

3.2 Effects of Location on the Roof

Results presented in section 3.1 indicate little variation in the force coefficients based on the location of the equipment on the roof. A further investigation of location effects was conducted using RME unit ACU7 (Vent Style 1) at three different locations on the roof. The three locations tested are 1-1, 2-2 and 3-3 as defined in Figure 4. At each location, the unit is mounted 0.14 m (0.46 ft) above the roof surface. Figure 18 depicts a summary of the force coefficients for each experimental configuration at the wind angle where the worst peak coefficient for each DOF occurred. Overall, there does not appear to be any clear trend where one location on the roof has higher or lower wind forces. The slight difference in the observed wind loads between locations appears dependent on which component is being considered. The data shows that when moving from location 1-1 to 3-3 there is a trend of increasing peak force coefficients for *CFx* and *CMy* and a trend of decreasing force coefficients for *CFy* and *CMx*. For both *CFz* and *CMz,* there does not appear to be any significant change based on location on the roof. However, it should be noted that the force balance locations used in the study are upstream of the point where flow separation that occurs at the edge of the roof reattaches to the roof. Therefore the flow regime at all locations where an RME was tested is similar. It is possible that the wind loads downstream of the reattachment point would exhibit a more significant difference but lower magnitude loads than the results presented in this report. The reduction in loads for areas farther from the edge of the building deserves further study. Similar to the results presented in section 3.1, the coefficients provided by ASCE7-10 (2010) envelope the measured wind loads obtained at all roof locations tested.

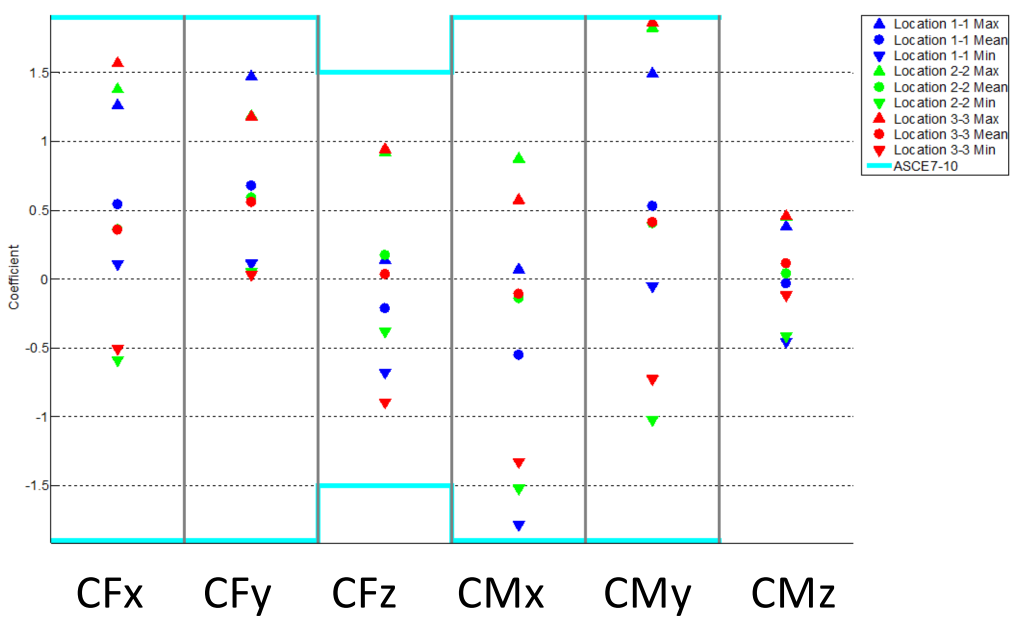

Figure 18: Summary of the max, min and mean coefficients for each degree of freedom for ACU7 mounted at an elevation of 0.14 m at three locations on the roof

3.3 Effect of Elevation

To evaluate the effects of elevation, ACU 5, ACU 7 and the box shown in Table 3 were elevated to three different heights above the roof surface using two platforms. The clearance height between the roof surface and the bottom of the RME, *h*, were 0.14 m (0.46 ft.), 0.3 m (1 ft.) and 0.61 m (2 ft.). Figure 19 shows an example of the two platforms used in the experiments to elevate ACU 7 to an *h* of 0.3 m (1 ft.) (left) and 0.61 m (2 ft) (right). Figure 20 presents the summary of the worst peak force coefficients for each DOF for ACU 5 at three different heights above the roof at location 1-1. In addition to results from tests at three elevations, results from another case where flow underneath the RME unit was blocked is also shown in Figure 20 and denoted in the legend as "blocked." Similarly, Figure 21 and Figure 22 present the effect of elevation for the box tested at location 1-1 and ACU 7 at location 2-2 respectively. For both ACU 5 and the box unit at location 1-1 there is a clear trend of increasing force coefficients with elevation above the roof for *CFx*, *CFy*, *CFz* and *CMx*. The increase is likely due to an increase in wind speed with height cause by the shear layer generated at the roof edge. Since the size of the separated region on the roof scales reasonably well with roof height, it is expected that the ratio of *h* to the height of the building, *H*, would be a critical parameter. The wind loads on ACU 7 at location 2-2 show no trend of increasing force coefficients with elevation over all DOF. This indicates that the location on the roof is also a critical parameter when examining the elevation of units above the roof deck. This finding is not surprising since the elevation of the shear layer above the roof will vary based on location on the roof. At an elevation of 0.61 m (2 ft.) the force coefficients of ACU5 are equal to those in the ASCE7-10 (2010), while the coefficients for the box exceed those in the ASCE7-10 (2010) by approximately 21 percent. These results suggest caution should be exercised when elevating RME that are located close to the edge of the buildings and that further refinement of section 29.5.1 in ASCE7-10 (2010) for wind loads on roof-mounted equipment may be necessary. The results suggest that applying different force coefficients and limits to the height of the equipment, *h*, above the roof based on roof zones (e.g. 'corner', 'edge' and 'interior' zones) is likely a more appropriate approach than universally increasing the force coefficients found in section 29.5.1 in ASCE7-10 (2010). Preventing flow underneath ACU 5 appears to increase *CFz* compared to the non-blocked case, while having little effect on the other DOF.

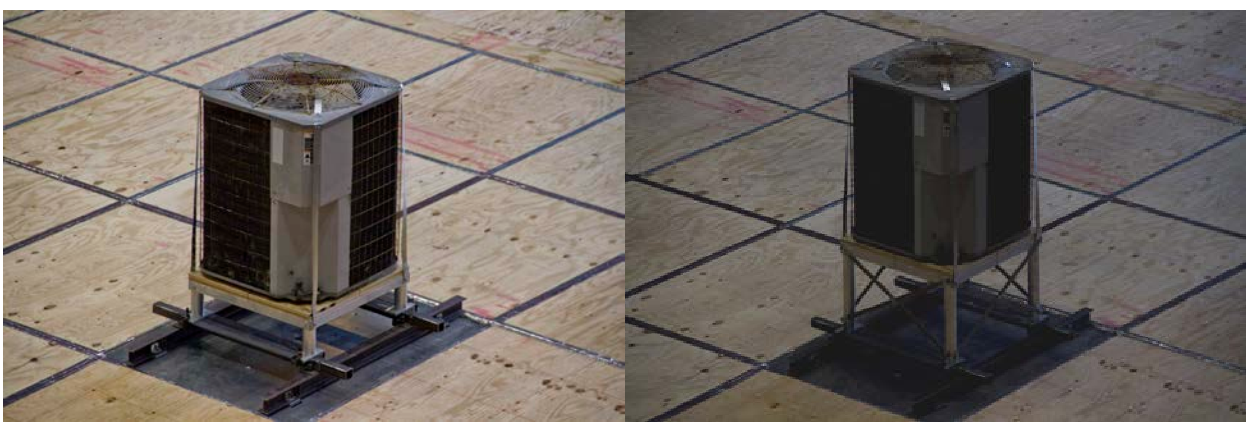

Figure 19: Example of ACU 7 elevated to two different heights (h) above the roof. (Left) h=0.3 m (1 ft.). (Right) h=0.61 m (2 ft.)

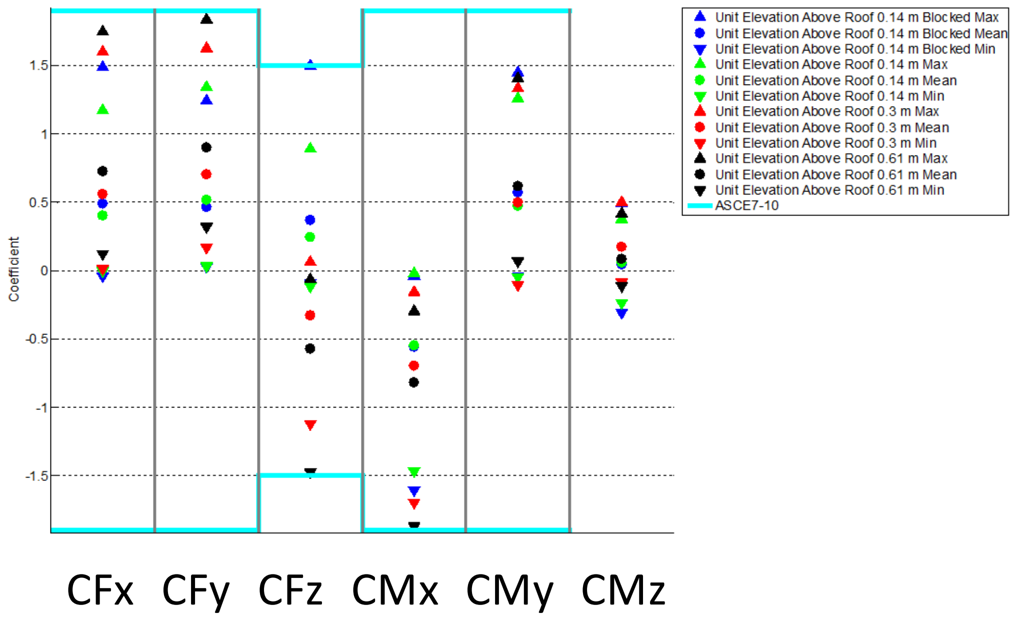

Figure 20: Summary of the max, min and mean coefficients for each degree of freedom for ACU5 mounted at different elevations above the roof at location 1-1

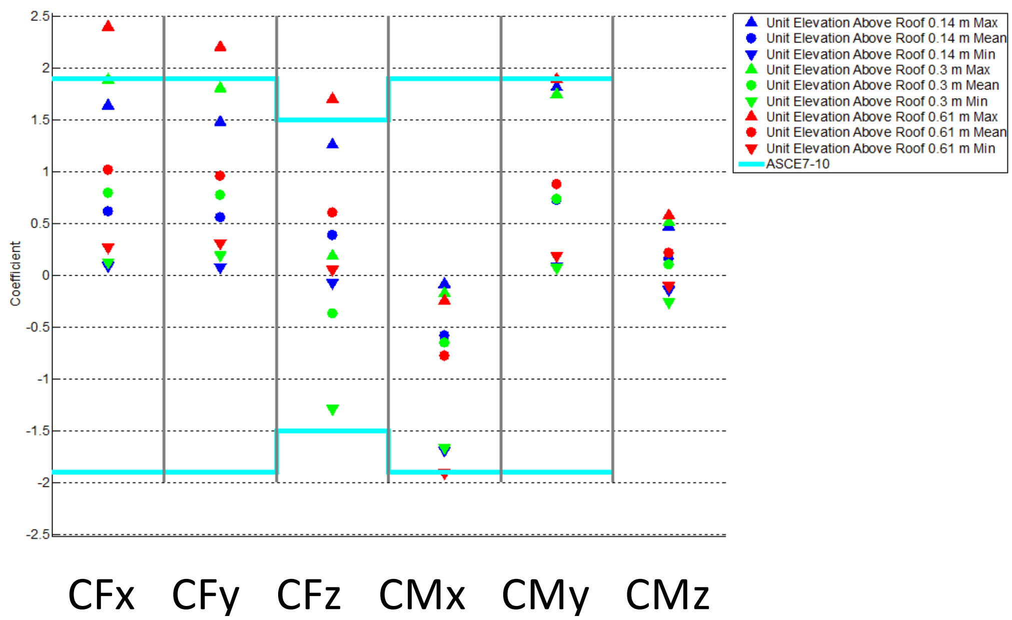

Figure 21: Summary of the max, min and mean coefficients for each degree of freedom for the box mounted at different elevations above the roof at location 1-1

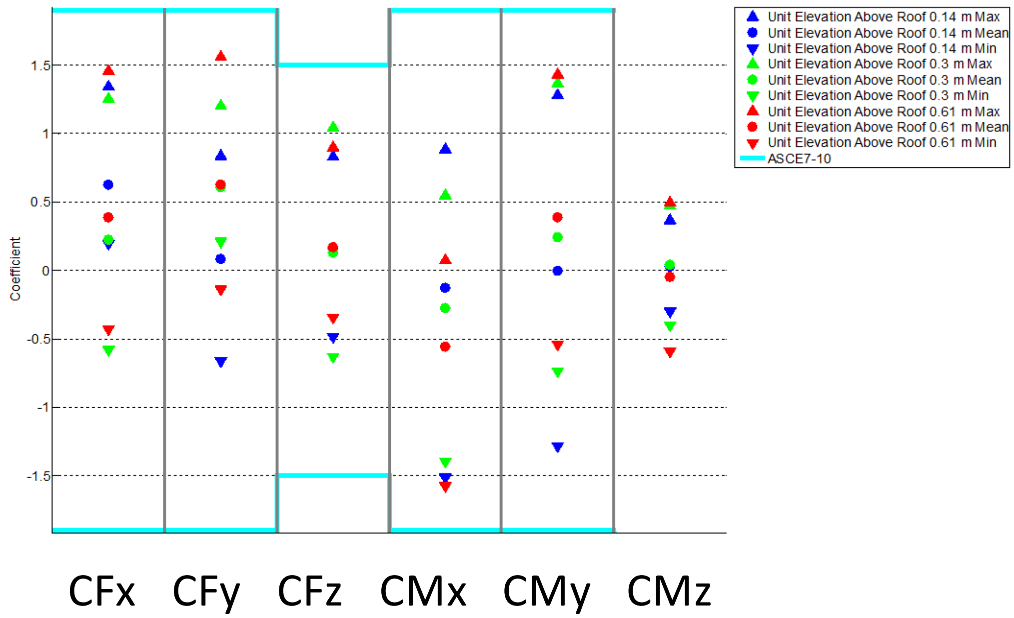

Figure 22: Summary of the max, min and mean coefficients for each degree of freedom for ACU 7 mounted at different elevations above the roof at location 2-2

3.4 Wind Loads on Goosenecks

Two goosenecks with heights of 1.5 m (5 ft.) were tested at locations 2-2 and 3-3. The first gooseneck had a circular cross-section with diameter 0.3 m (1 ft.), while the second had a rectangular cross section of 0.3 x 0.46 m (1 x 1.5 ft.). Figure 23 shows the rectangular cross section gooseneck mounted on the roof of the test building at location 3-3. Figure 24 through Figure 29 present the maximum, minimum and mean coefficients for each DOF versus wind angle for each gooseneck at the two locations on the roof. A good collapse is observed for the rectangular and circular goose neck vents and the two test locations for *CFx*, *CFy*, *CMx* and *CMy*. This further emphasizing the conclusion of section 3.2 that the location of the equipment on roof does not substantially alter the wind loads within the locations tested in the study. In general, the rectangular gooseneck experiences larger loads than the circular gooseneck.

For both goosenecks the mean coefficients of *CFx*, *CFy*, *CMx* and *CMy* follow the same trend with wind angle as the smaller air-conditioning units (ACU5, ACU7, Box) shown in Figures 10, 11, 13 and 14. However, unlike the smaller air conditioning units the peak coefficients for the gooseneck vents decrease in magnitude from a wind angle of 0° to a wind angle of approximately 60° then show an increase in magnitude from 60° to 90°. This apparent "U" shape in the peak wind loads in largely cause by the change of the projected area of the goosenecks. This trend can be observed in Figures 10, 11, 13, 14 for smaller air-conditioning units. However, it is much less apparent than with the gooseneck vents. Due to the shape of the gooseneck vents, the projected area of the goose necks varies substantially with wind angle. For example, the projected area of the rectangular gooseneck goes from a minimum of 0.46 m^2 (1.5 ft^2) at 0° to a maximum of 0.99 m^2 (3.3 ft^2) at 60°, back to 0.88 m^2 (2.9 ft^2)at 90°. In contrast, the largest change in projected area for the air-conditioning units is from an area of 0.7 m^2 to 1 m^2, for

ACU5. Since the flows on the roof – particularly in the separated region – vary substantially with wind angle, it is not surprising that the projected area of the unit does not offer a good collapse of the data. It should be noted that unlike the smaller air-conditioning units the centroid of the goosenecks changes with the change in projected area due to their asymmetric shape with height. The change of the centroid position changes the distance *L*, used to normalize *CMx* and *CMy* by approximately 18 percent. Similarly, the distance *L*, for CMz also increases from 0.1524 m (0.5 ft) at 0° to a maximum of 0.9144 m (3 ft) at 90°. The effect of increasing *L* with wind angle is clearly apparent in Figure 29.

Figure 30 presents a summary of the peak force coefficients on both goosenecks at the two locations tested. The peak force coefficients on the goosenecks are significantly larger than those observed for other RME examined in the study, while the mean coefficients are similar in magnitude to the other RME. The large spread of the data between peak positive and negative data at the same wind angle suggests that these large peak coefficients may be the result of significant vibration of the goosenecks. This seems possible since the goosenecks are by far the least stiff RME elements tested. Table 4 presents the absolute peak coefficient for each DOF for each wind angle for the gooseneck vents. In Table 4 numbers colored in red indicate that the force coefficient exceeds the *GCr* coefficient provided by ASCE7-10 (2010), while purple numbers represent force coefficients that are with 15 percent of the ASCE7-10 (2010) *GCr* coefficients. As shown in both Figure 30 and Table 4 the measured coefficients exceed those specified by ASCE7-10 (2010) in some cases by as much as 85 percent. However, as shown in Table 4 the critical angle in which the peak wind load occurs is predominately 0° where the projected area is smallest. In addition, with the exception of *CFz* the coefficients for all DOF do not exceed those in the ASCE7-10 (2010) for wind angles between 30° and 75°. This is contrary to other RME equipment where the critical wind angle clearly varied for each DOF (as shown in Figure 10 through Figure 15). These results suggest that using the projected area in the perpendicular to the wind direction for high aspect ratio or asymmetric RME may not be the best normalization. Moreover, given the large spread in the data a more detailed investigation into the forces on goosenecks, particularly examining the vibration of these units seems prudent.

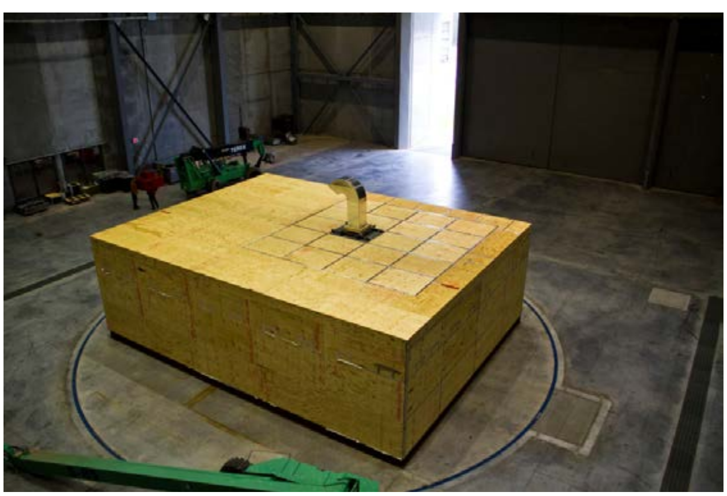

Figure 23: Photograph of the square cross section gooseneck at location 3-3

Table 4: Summary of the absolute value of the peak force coefficients for each DOF. Red numbers indicate that the peak coefficient exceeds the ASCE7-10 value, while purple numbers indicate that the peak coefficient is within 15percent of the ASCE7-10 value

	Wind Angle							**Critical Angle**
Location 2-2	**0**	**15**	**30**	**45**	**60**	**75**	**90**	
Rectangular Gooseneck *CFx*	**2.30**	**1.67**	1.42	1.17	0.95	1.01	1.15	0
Rectangular Gooseneck *CFy*	**2.24**	**1.75**	1.06	1.29	1.43	1.56	**1.71**	0
Rectangular Gooseneck *CFz*	1.16	0.90	0.54	0.52	0.51	1.14	1.11	0
Rectangular Gooseneck *CMx*	**2.87**	**2.07**	0.99	1.21	1.47	**1.87**	**2.05**	0
Rectangular Gooseneck *CMy*	**2.48**	**1.64**	1.06	0.94	0.74	1.05	1.20	0
Circular Gooseneck *CFx*	1.36	1.19	1.14	1.11	0.99	1.56	**1.62**	90
Circular Gooseneck *CFy*	**1.98**	**1.64**	1.10	1.02	1.12	1.16	1.21	0
Circular Gooseneck *CFz*	1.16	1.10	1.27	1.43	**1.53**	**2.80**	**2.61**	75
Circular Gooseneck *CMx*	**2.73**	**2.36**	1.18	1.02	1.14	1.24	1.45	0
Circular Gooseneck *CMy*	**1.67**	1.28	0.98	0.98	0.88	1.51	**2.00**	90
Location 3-3								
Rectangular Gooseneck *CFx*	**2.39**	**1.73**	1.40	1.12	0.87	1.03	1.25	0
Rectangular Gooseneck *CFy*	**2.66**	**1.92**	1.10	1.23	1.40	1.43	1.57	0
Rectangular Gooseneck *CFz*	**1.83**	1.14	0.53	0.86	1.10	**1.60**	**1.73**	0
Rectangular Gooseneck *CMx*	**2.80**	**1.75**	0.92	1.10	1.19	1.46	**1.67**	0
Rectangular Gooseneck *CMy*	**2.38**	**1.68**	1.13	1.05	0.83	1.12	1.38	0
Circular Gooseneck *CFx*	1.48	1.26	1.02	0.96	0.86	1.42	1.59	90
Circular Gooseneck *CFy*	**1.62**	**1.63**	0.92	0.98	1.09	1.23	1.19	15
Circular Gooseneck *CFz*	**1.76**	**2.00**	1.02	0.87	0.72	**1.92**	**1.59**	15
Circular Gooseneck *CMx*	**1.96**	**1.78**	0.89	0.80	0.92	1.13	1.26	0
Circular Gooseneck *CMz*	**1.67**	1.28	0.91	0.82	0.77	1.36	**1.66**	0

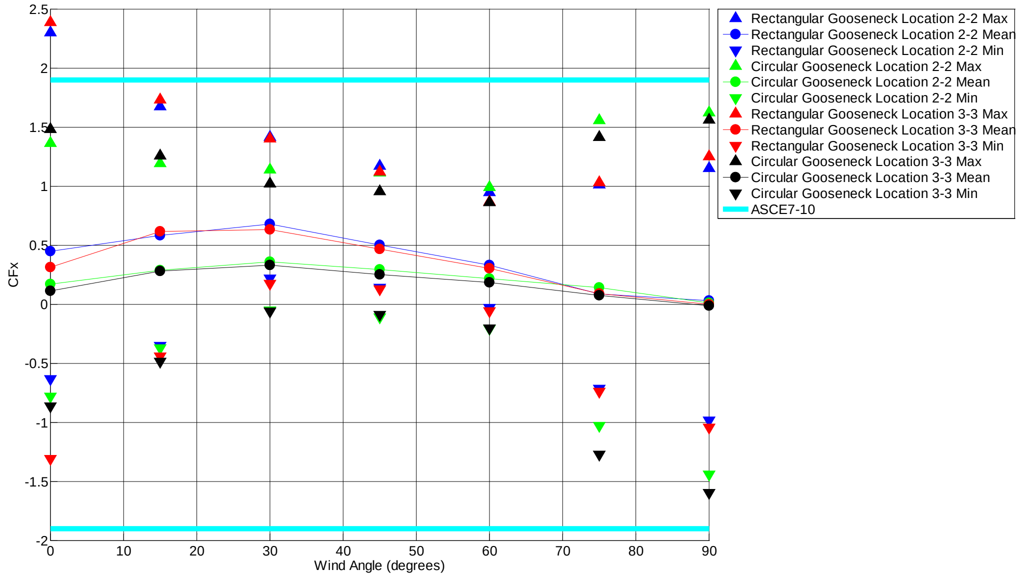

Figure 24: *CFx* along wind force coefficients for gooseneck vents

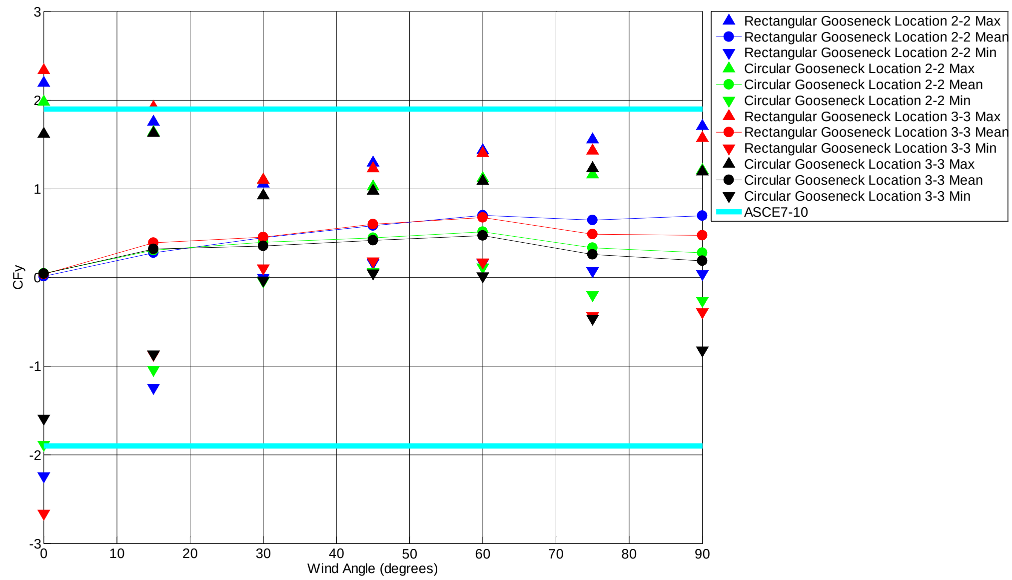

Figure 25: *CFy* lateral force coefficients for gooseneck vents

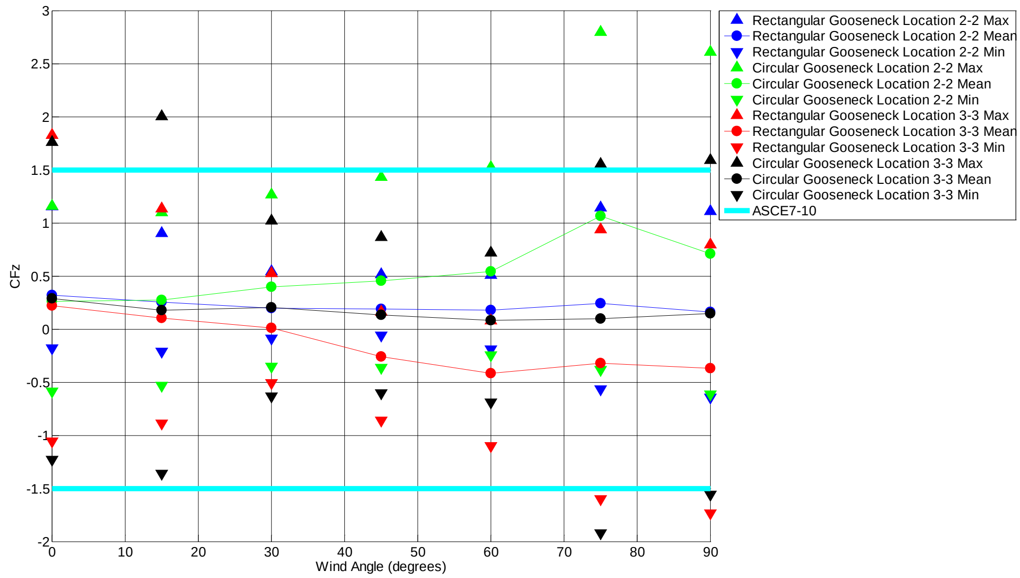

Figure 26: CFz vertical force coefficients for gooseneck vents

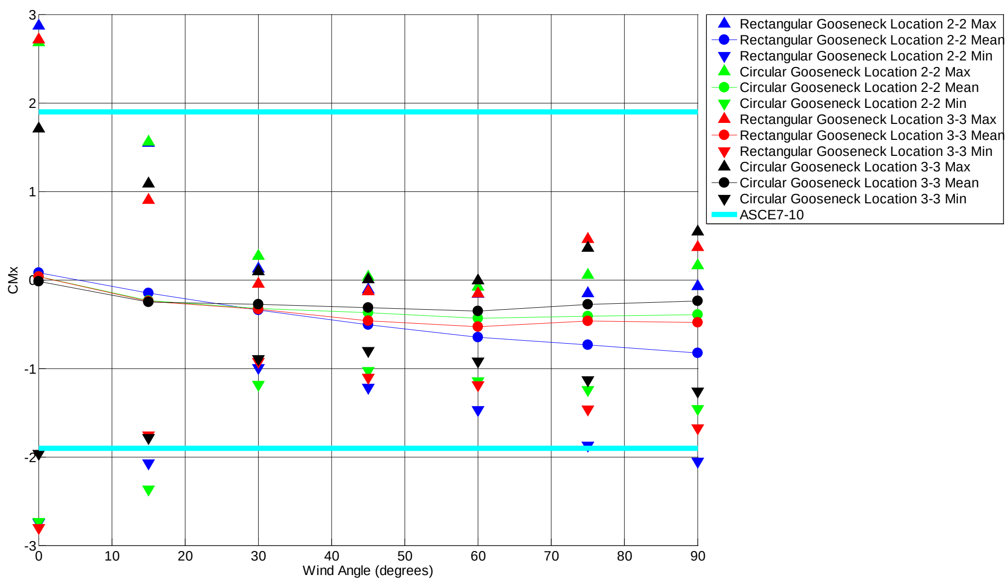

Figure 27: *CMx* moment coefficients for gooseneck vents

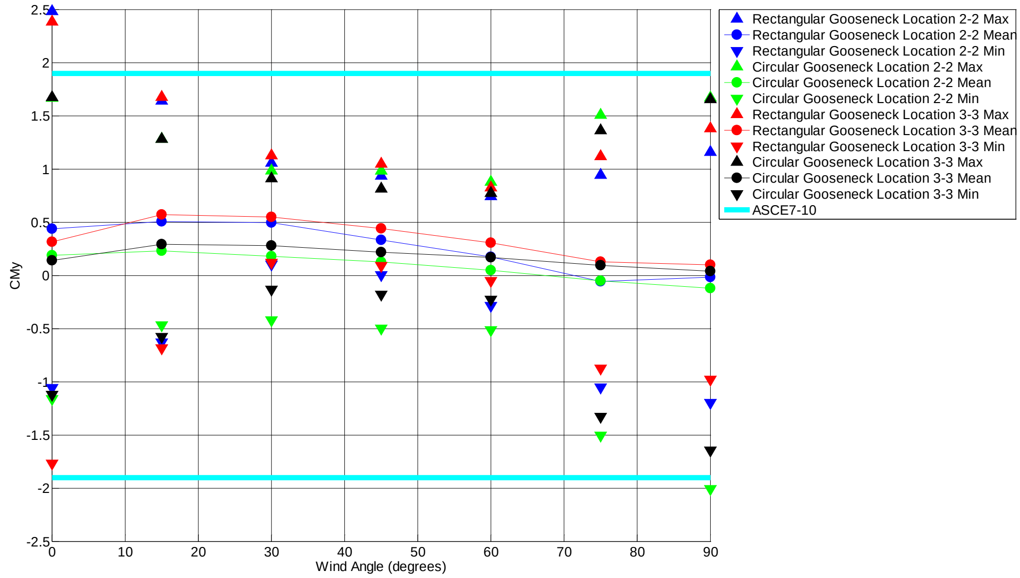

Figure 28: *CMy* moment coefficients for gooseneck vents

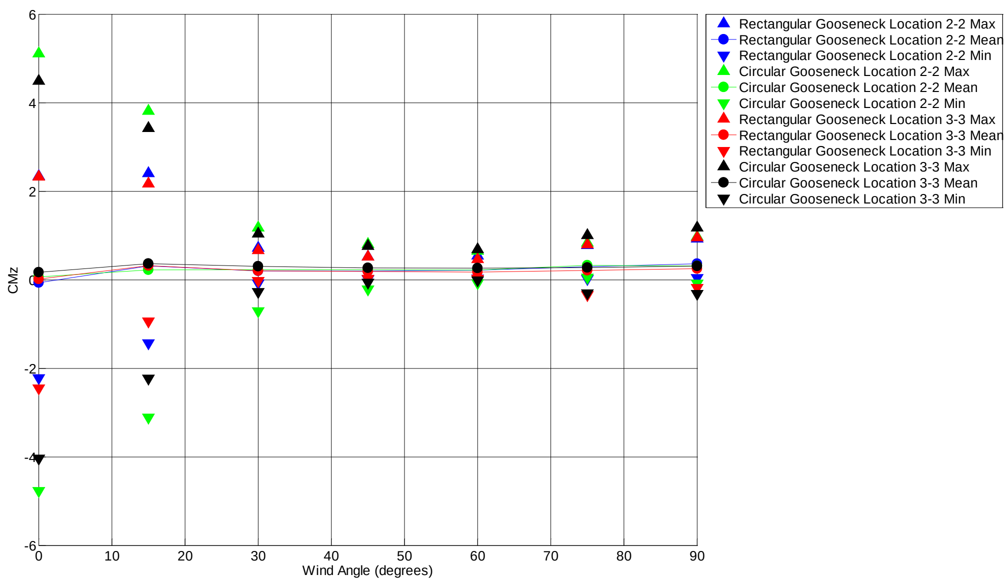

Figure 29: *CMz* moment coefficients for gooseneck vents

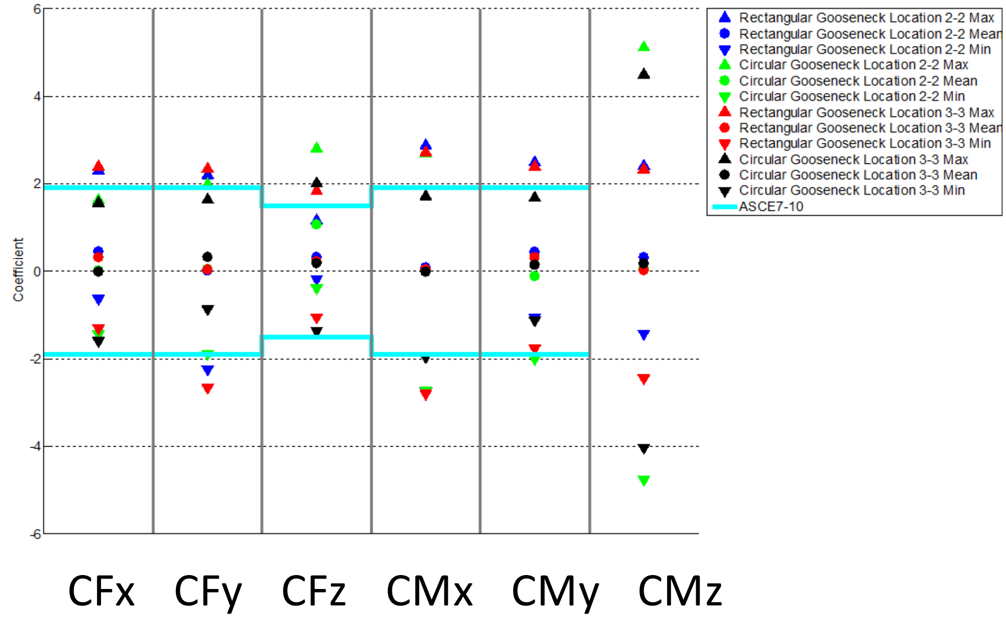

Figure 30: Summary of the max, min and mean coefficients for each degree of freedom for both square and circular goosenecks at locations 2-2 and 3-3.

3.5 Point of Lateral Force Application and Effects of Unit Size

Overturning moments that must be resisted by the anchorage of the RME are created by lateral forces applied to the units. The actual magnitudes of the overturning moments depend on the magnitude of the lateral forces and how they are distributed over the surface of the units. For simple engineering calculations, this is reduced to a force that is applied at some height above the base of the unit. For the coordinate system used to define the forces and moments, +*Fx* creates a +*My* and +*Fy* creates a -*Mx*. If +*Fx* multiplied by L, the height of the centroid of the projected area of the unit in the vertical plane perpendicular to the wind direction, is substituted for *My* in Equation 7 the right hand side of the equation becomes the same for *CFx* and *CMy*. Consequently, if +*CFx* is equal to *CMy* then the lateral force can in fact be assumed to be applied at the centroid of the projected area. Similarly, if *CFy* and -*CMx* are equal the force in the y-direction can be assumed to be applied at the centroid of the projected area. Figure 31 (left) plots mean *CFy* versus mean *CMx* for all RME configurations and wind direction presented in sections 3.1 through 3.4 while Figure 31 (right) presents the same comparison only between mean *CFx* and *CMy*. In both plots of Figure 31 the scatter of the measured values fall on the diagonal line with a slope of ±1 (black line shown in Figure 31). This shows that the assumption that the lateral force should be applied at the centroid of the vertical projected area is appropriate when calculating the over turning moments from the coefficients provided in the ASCE7-10 (2010).

All equipment tested as part of this study had a projected area of less than five percent of the smallest building wall area. ASCE7-10 (2010) includes provisions for the reduction in forces as the area of the RME increases beyond 10percent of the wall or roof area. Because the units tested were so small, it is not possible to use data from this study to explore the ASCE7-10 (2010) load reduction provisions.

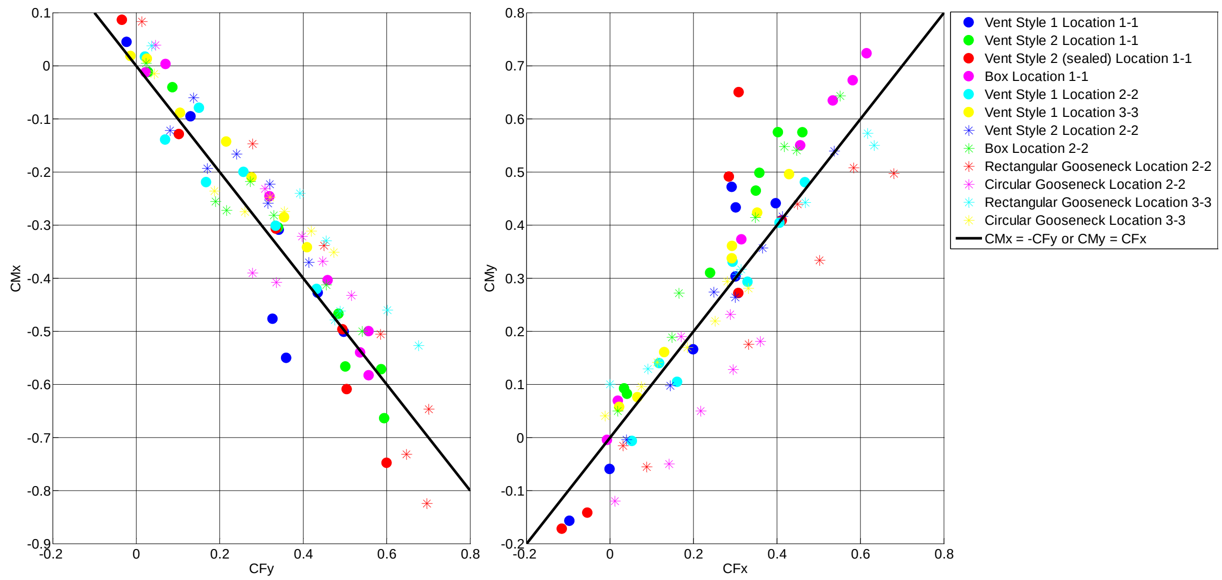

Figure 31: Comparison of *CFy* to *CMx* (left) and *CFx* to *CMy* (right) for RME cases presented in sections 3.1 to 3.4.

3.6 Effect of Multiple Units (Shielding)

In real-world installations of RME, several units are often installed in close proximity to each other. Several experiments were conducted to investigate the effect of having multiple RME in close proximity. Figure 32 shows ACU 7 at location 2-2 surrounded on two sides by four similarly sized units. The spacing between units ranged from 0.38 m to 0.76 m and all surrounding units were elevated 0.14 m above the roof surface. With the position of the surrounding units kept constant, the loads on ACU 7 were tested at three different heights above the roof, i.e. *h*=0.14 m (0.46 ft.), *h*=0.3 m (1 ft.) and *h*=0.62 m (2 ft.). The summary of the peak wind loads for each DOF at each height is shown in Figure 33 along with the peak loads from ACU 7 at location 2-2 when no surrounding units are present (isolated). When comparing the isolated case to the surrounded case at *h*=0.14 (0.46 ft.) there is a substantial reduction in the wind loads for all DOF with the exception of *CMz* which appears to be largely unaffected by the presence of the surrounding units. The amount of load reduction varies from -0.1percent for *CMz* to 70percent for *CMy*. The peak force coefficients for ACU 7 increase with increasing elevation. An increase based on elevation above the roof would be expected given the finding from section 3.3 and intuitively since the unit is being elevated above the surrounding units. At *h*=0.61 m (2 ft.) where 63percent of the unit is unshielded, the force coefficients in Figure 33 remain lower than their isolated counter parts presented in Figure 22 for *CFx*, *CFy* and *CMy*. However, *CMx* is about equal to or slightly larger than the value for the unshielded case.

The findings are similar to those presented by Erwin et al. (2011) where substantial load reductions on RME were observed due to screens. The use of architectural screens is often a requirement of many urban planning and zoning departments. However, building code provisions do not provide any guidance on these potential reductions. In fact ASCE 7-10 (2010) includes language in Section 29.1.4 regarding shielding that can be interpreted as prohibiting the use of reductions due to shielding. While this language was intended to prevent engineers from arbitrarily reducing wind loads due to effects of surrounding buildings and other structures or terrain features, the code does recognize the reductions in roof loads associated with parapets and effects of shielding, with some limitations on the amount of reductions allowed, that are routinely accounted for in site specific boundary layer wind tunnel tests. The results suggest that a substantial load reduction may be achieved through shielding, either by surrounding units or screen wall. Consequently, it is recommended that a much more rigorous study into the effects of shielding be undertaken to both confirm the results and potentially allow for the codification of load reduction factors associated with screens or barriers enclosing a single unit or a cluster of units.

In addition to the RME at location 2-2 the loads on ACU5 and ACU6 at locations 1-1 and 2-1 were also measured. The summary for the peak loads for each DOF is shown in Figure 34 and Figure 35 for location 1-1 and 2-1 respectively for the three elevations of ACU7 at location 2-2. In general the elevation of ACU7 at location 2-2 has a negligible effect on the loads for both ACU5 and ACU6 at locations 1-1 and 2-1. Figure 34 also presents a comparison between results for ACU5 at location 1-1 when surrounding units are present versus when ACU5 is isolated on the roof. While the match between the surrounded and isolated cases is not perfect, there is no clear increase or decrease of the wind loads on ACU5 at location 1-1 when the surrounding units are present.

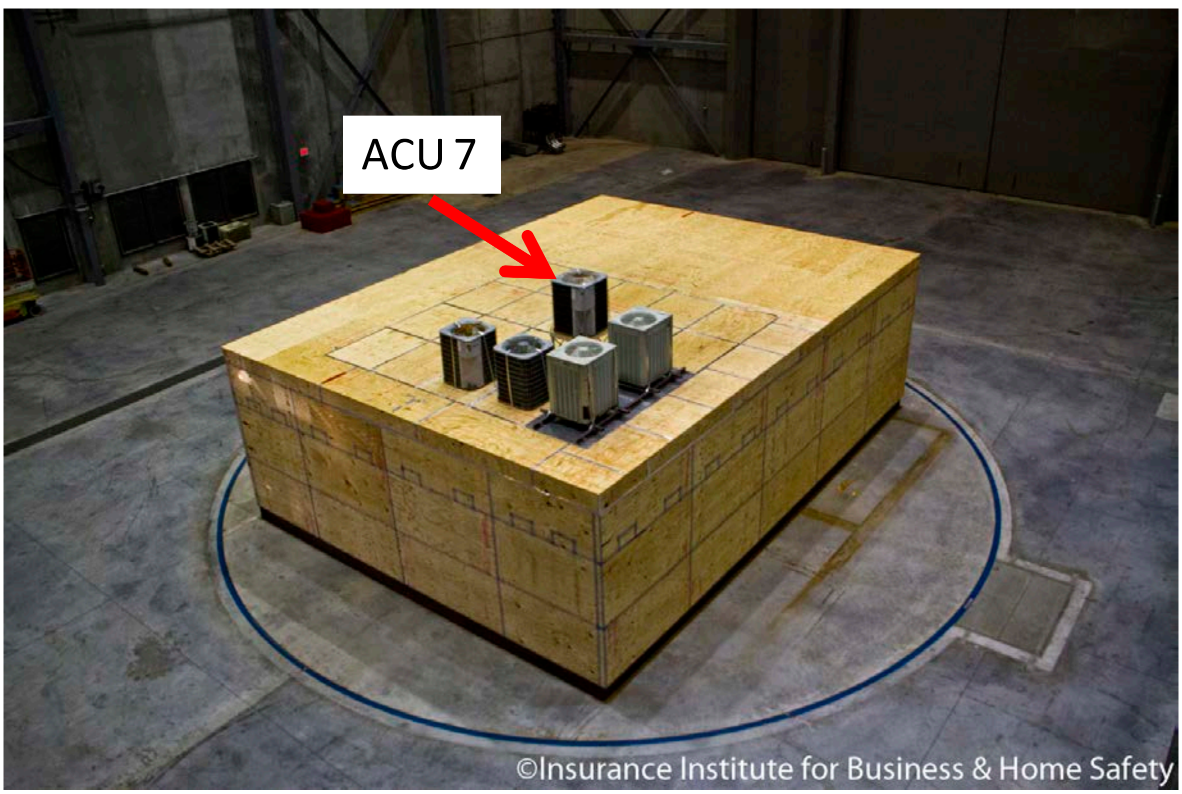

Figure 32: Photograph of ACU 7 at location 2-2 surrounded by other RME

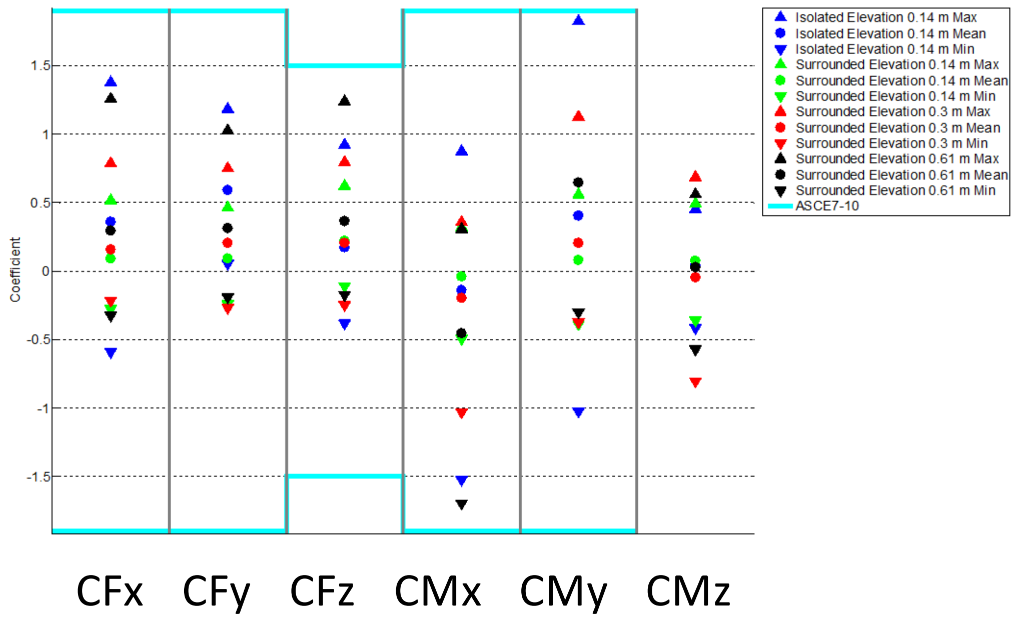

Figure 33: Summary of the max, min and mean force and moment coefficients for ACU 7 at location 2-2 for various elevations above the roof surface when surrounded by other RME units.

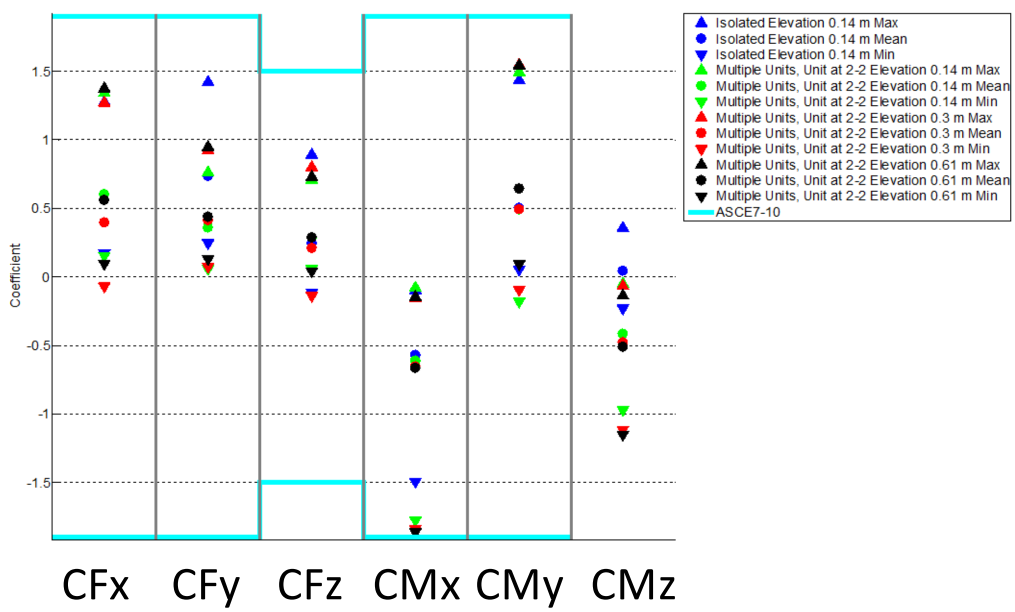

Figure 34: Summary of the max, min and mean force and moment coefficients for ACU 6 at location 1-1 when multiple units are present and unit ACU 7 at location 2-2 is installed at different elevations.

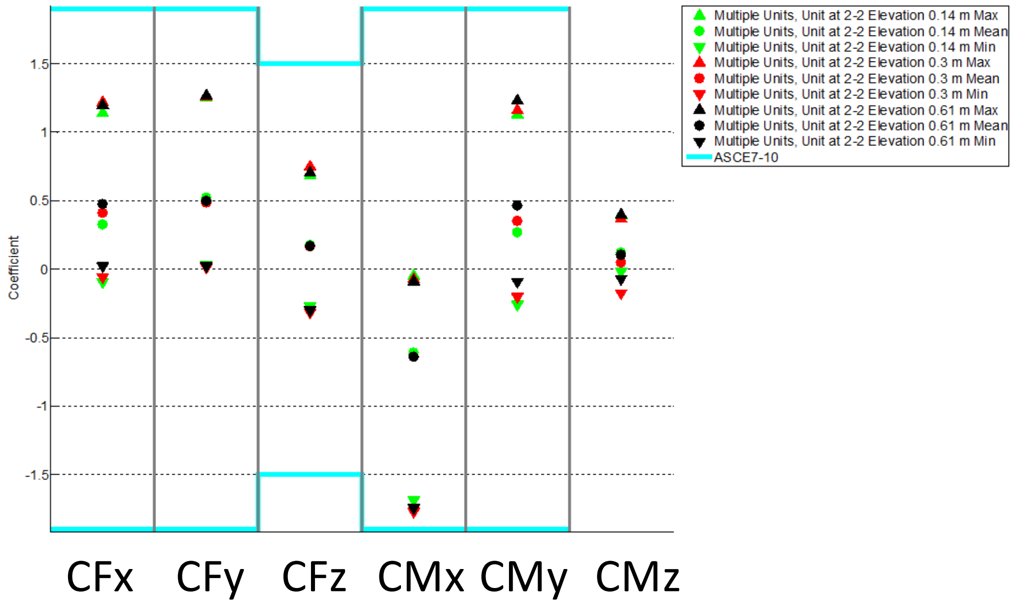

Figure 35: Summary of the max, min and mean force and moment coefficients for ACU 6 at location 2-1 when multiple units are present and unit ACU 7 at location 2-2 is installed at different elevations.

4 Conclusions

The following conclusions can be drawn from results of the investigation into the wind loads on various types of roof-mounted equipment:

- The wind loading coefficients in the ASCE7-10 (2010) are adequate to envelope the wind loads obtained from all RME configurations in the study, with the exception of goosenecks and at certain locations where the RME is substantially elevated above the roof surface.
- The ASCE7-10 (2010) wind load coefficients are conservative, but do not appear to be overly conservative.
- The type of venting style or fin style does not appear to have a large effect on the wind loads. Modeling RME – as a solid rectangle – generated higher vertical force coefficients *CFz*, while all other forces and moments appeared unchanged, as compared to the vented RME. The results suggest model scale wind tunnels, which typically model RME as a solid rectangle, may overestimate the uplift forces, *CFz,* for vented condenser units.
- Increasing the elevation of the RME above the roof surface increases wind loads for locations on the roof and range of elevations tested in the study. Based on the hypothesis that this increase results from the unit experiencing higher wind speeds in the separated shear layer, wind loads can be expected to reach some maximum at a certain ratio between the height above the roof and the height of the building. Moreover, it has been shown that the increase of force coefficients with elevation above the roof is less at locations closer to the interior of the roof, as compared to locations close to the roof edge. As a result, codification applying different force

coefficients and limits to the height of the equipment, *h*, above the roof based on roof zones (e.g. corner, edge and interior zones) is likely a more appropriate approach than universally increasing the force coefficients found in section 29.5.1 of ASCE7-10 (2010).

- Results suggest, on average, the measured overturning moments are equal to what would be expected if the lateral forces are applied at the centroid of the projected area of the unit in a vertical plane perpendicular to the wind direction. The ASCE7-10 (2010) does not explicitly state where the force coefficients should be applied for calculating overturning moments on the RME. Based on the results, language should be added to the ASCE7-10 (2010) stating that the wind loads be applied at the centroid of the RME.
- For the gooseneck units, the projected area varies significantly based on wind angle. For these high aspect ratio units with an asymmetric geometry, the results suggest that projected area may not be the appropriate area for the normalization of the applied forces. However, a significantly more detailed study on these types of units would be required to confirm this conclusion.
- A significant reduction in wind loads on RME was observed for units downstream of a cluster of units. The reduction has been found to be as high as 70 percent for the downwind unit. However, upwind units did not experience a significant reduction in loads. The magnitude of reductions in loads for shielded units appear consistent with previous results from Erwin et al. (Erwin, 2011). With such a substantial decrease in wind loads due to shielding effects, a more detailed investigation appears warranted regarding shielding schemes using screens and barriers surrounding a unit or a cluster of units appears warranted.

5 Future work

The investigation studied a large number of RME configurations. However, certain aspects of the wind loads on RME deserve further study:

- Large load reductions were observed due to shielding effects from surrounding RME elements. The substantial reduction in wind loads observed from this shielding call for a more comprehensive investigation to quantify the shielding effects from screens and barriers.
- The wind loads on goosenecks were found to be substantially higher than for other RME elements. The goosenecks used in the study where quite tall, being nearly 40 percent of the overall building height. A rigorous investigation into the wind loads on goosenecks is warranted to confirm the high wind loading coefficients observed in the study. In addition, a more detail study of RME with high aspect ratios and asymmetric geometries is required to determine if the projected area perpendicular to the wind direction is the correct normalization area.
- Experiments revealed that the forces on nearly all RME elements were measured with the units mounted in the separated flow region near the upwind edges of the roof. This means that the units were located upstream of the flow reattachment point. The wind loads on RME in the interior region of the roof downstream of the flow reattachment point deserves further study.

- Parapets along the edges of the roof are common. Since the investigation did not examine the effect of parapets, this should be examined in future investigations.

6 References

American Society of Civil Engineers (ASCE 7-10). (2010). *Minimum Design Loads for Buildings and Other Structures*. Reston, Virginia: American Society of Civil Engineers.

Engineering Data Science Unit (ESDU). (1982). *Strong winds in the atmosheric boundary layer Part 1: mean-hourly wind speeds*. Data Item 82026.

Erwin, J.W., Chowdhury, A.G. & Bitsuamlak, G. (2011). Wind loads rooftop equipment mounted on a flat roof. *Journal of Wind and Engineering*, 8(1), 23-42.

Federal Emergency Management Agency (FEMA). (2006). *Hurricane Katrina in the Gulf Coast Mitigation Assessment Team Report Building Performance Observations, Recommendations, and Technical Guidance.* FEMA 549.

Hosoya, N., Cermak, J.E. & Steele, C. (2001). A wind-tunnel study of a cubic rooftop ac unit on a low building. *1st Americas Conference on Wind Engineering*, Clemson, SC, USA.

Kopp, G.A. & Traczuk, G. (2007). *Wind Loads on Roof-Mounted Cube* (BLWT-SS47-2007). London, ON, Canada: The Boundary Layer Wind Tunnel Laboratory.

Liu, Z., Brown, T.M., Cope, A.D. & Reinhold, T.A. (2011). Simulation Wind Conditions/Events in the IBHS Research Center Full-Scale Test Facility. *13th International Conference on Wind Engineering,* Amsterdam, Netherlands.

Morrison, M.J., Brown, T.M. & Liu, Z. (2012). Comparison of Field and Full-Scale Laboratory Peak Pressures at the IBHS Research Center. *ATC&SEI Advances in Hurricane Engineering Conference*, Miami, FL, USA.

Smith D. (2010). *Validation of Wind and Wind-Induced Pressure Data Collected at the Institute for Building and Home Safety's State-of-the-Art Multi-Peril Applied Research and Training Facility*. Lubbock, TX, USA: Wind Science and Engineering Research Center.

St. Pierre, L.M., Kopp, G.A., Surry, D. & Ho, T.C.E. (2005). The UWO contribution to the NIST aerodynamic database for wind loads on low buildings: Part 2. Comparison of data with wind load provisions. *Journal of Wind Engineering and Industrial Aerodynamics*, 93, 31-59. doi:10.1016/j.jweia.2004.07.007

APPENDIX A Load Cell Serial Numbers in Each Force Balance

Figure 36 shows a drawing and dimensions of the force balance design along with the location of the 7 loads cells, LC1 through LC7. Table 5 through Table 7 provides the serial number, location and range for the loads cells located in each force balance.

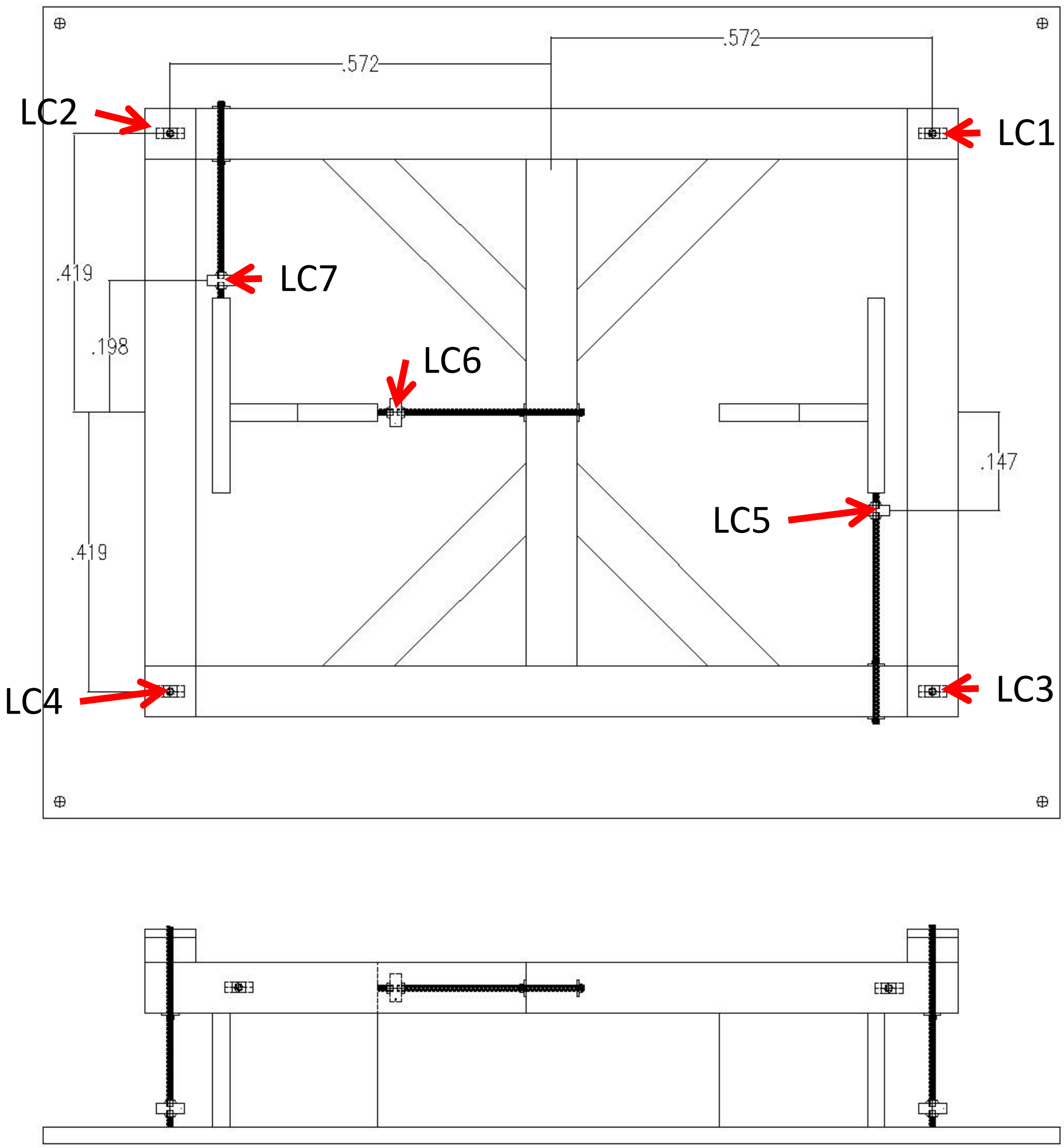

Figure 36: Drawing of the force balance design and location of loads cells LC1 through LC7. All dimensions are in meters

Table 5: Load cells located in force balance 1

Load Cell Serial #	Range N (lbs)	Location
261790	2230 (500)	LC1
263271	2230 (500)	LC2
263270	2230 (500)	LC3
261789	2230 (500)	LC4
260350	892 (200)	LC5
260351	892 (200)	LC6
260352	892 (200)	LC7

Table 6: Load cells located in force balance 2

Load Cell Serial #	Range N (lbs)	Location
261915	2230 (500)	LC1
261916	2230 (500)	LC2
261785	2230 (500)	LC3
261788	2230 (500)	LC4
260344	892 (200)	LC5
260347	892 (200)	LC6
260349	892 (200)	LC7

Table 7: Load cells located in force balance 3

Load Cell Serial #	Range N (lbs)	Location
261786	2230 (500)	LC1
274765	2230 (500)	LC2
274766	2230 (500)	LC3
274767	2230 (500)	LC4
260346	892 (200)	LC5
260348	892 (200)	LC6
260345	892 (200)	LC7

APPENDIX B Calibration Matrix *M* for all three force balances

Table 8 through Table 10 provide the calibration matrices for force balances 1, 2 and 3 respectively. Figure 37 through Figure 39 present the percent error on full scale range for each DOF for each force balance. In general, for all DOF for all force balances the errors are not randomly distributed and tend to increase with increasing applied force. This trend is likely due to the deflection of the loading post at higher loads. Overall, with the exception of force balance unit 3 that exhibited a relatively large error in *CFy* at large lateral loads (1.5percent of full scale range), the errors in force balance measurements of forces are always less than 0.4percent of the full scale range and the errors in force balance measurements of moments are always less than 0.8percent of the full scale range. Errors are typically lower than these limits for most DOF at moderate loads.

Table 8: Solution matrix "*M*" for force balance 1 output in N for forces and Nm for moments

	Fx	*Fy*	*Fz*	*Mx*	*My*	*Mz*
	0.0662	0.0084	4.3575	-2.0050	-2.7263	0.0347
	-0.0438	-0.0437	4.9209	-1.5668	2.7888	-0.0211
	-0.0608	0.1292	4.8225	1.9122	-2.3513	-0.0355
	0.0414	0.0081	4.2961	1.8011	2.3841	-0.0255
	-0.0123	4.6546	0.0035	-0.5592	0.0038	2.3875
	4.8402	0.1325	0.6020	0.2240	0.9361	0.0127
	-0.0250	-4.5842	1.0570	1.0324	0.6505	2.3359

Table 9: Solution matrix "*M*" for force balance 2 output in N for forces and Nm for moments

	Fx	*Fy*	*Fz*	*Mx*	*My*	*Mz*
	0.0661	0.0407	4.7741	-1.9058	-2.6174	-0.0202
	0.0184	-0.0871	4.4842	-1.8743	2.5641	0.0301
	0.0132	0.0117	4.3903	1.8287	-2.5970	0.0209
	0.0108	0.0038	4.6353	1.9089	2.5730	-0.0072
	0.0172	4.9023	-0.1958	-0.5172	0.0692	2.5619
	4.9047	0.0913	-0.0315	-0.0208	0.5329	-0.0363
	0.0849	4.7015	0.1170	-0.5325	0.0031	-2.3422

Table 10: Solution matrix "*M*" for force balance 3 output in N for forces and Nm for moments

	Fx	*Fy*	*Fz*	*Mx*	*My*	*Mz*
	-0.1898	-0.0270	4.7471	-1.8245	-2.5595	-0.0265
	-0.0805	0.0366	4.4372	-1.9262	2.5360	0.0191
	0.1557	0.0299	4.3517	1.8253	-2.6392	-0.1485
	-0.0050	-0.0013	4.6748	1.9228	2.5993	-0.0048
	-0.0888	4.8669	-0.2349	-0.5335	0.0076	2.5086
	5.0086	0.0552	0.0149	0.0273	0.5336	-0.0776
	-0.0714	-4.6527	-0.1242	0.4898	-0.0312	2.4463

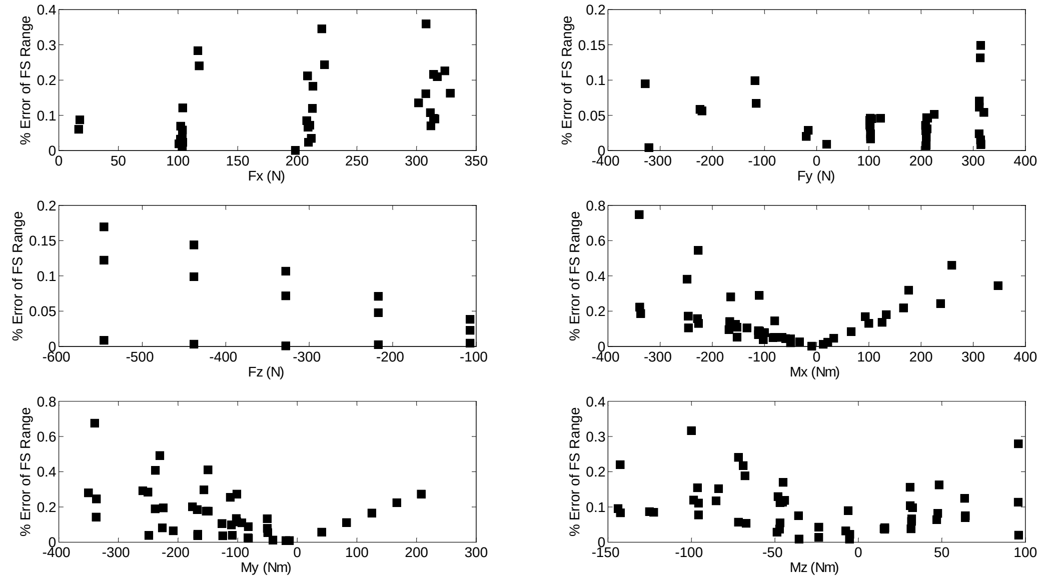

Figure 37: Errors as a percentage of full scale range for each DOF for force balance 1

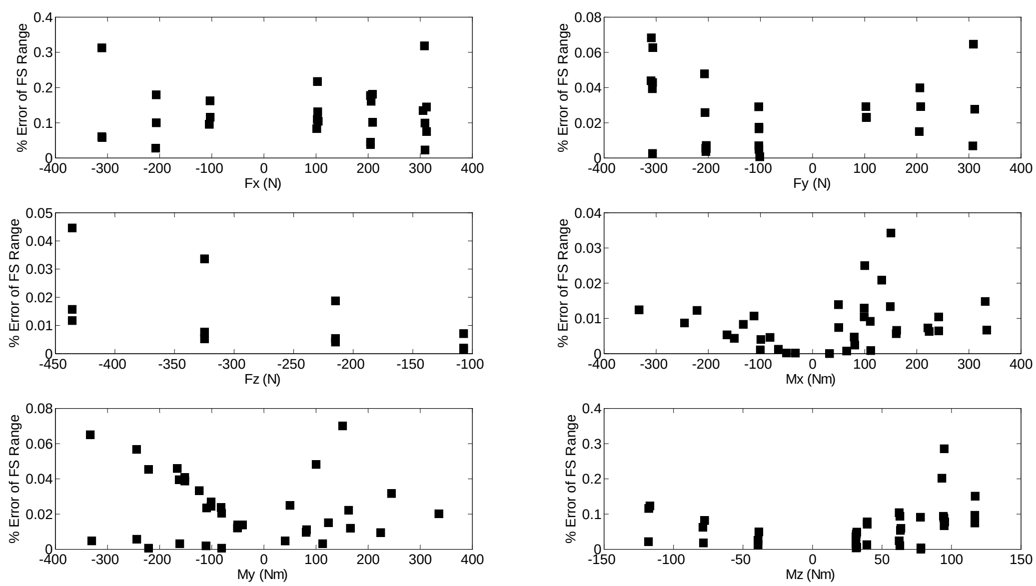

Figure 38: Errors as a percentage of full scale range for each DOF for force balance 2

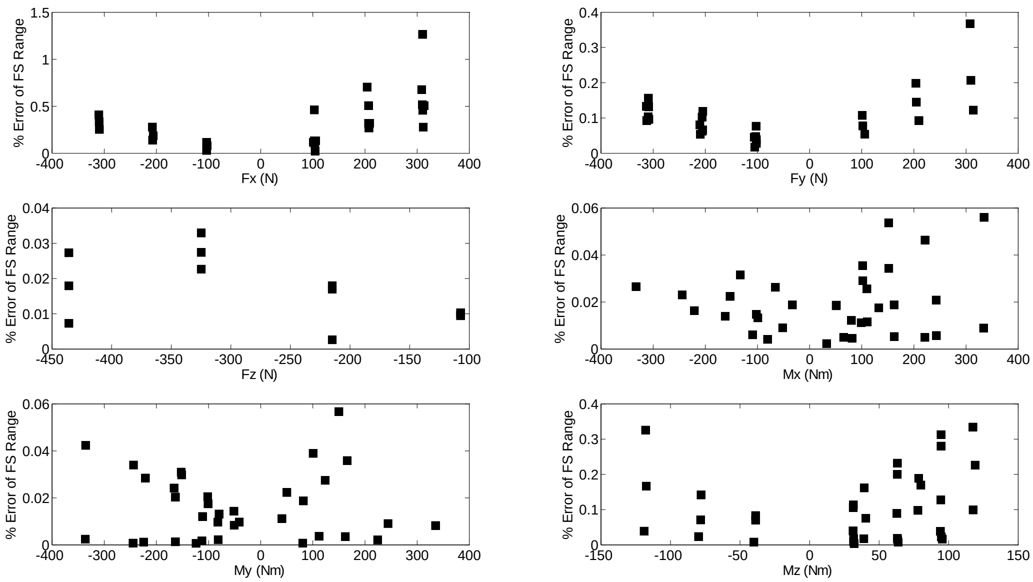

Figure 39: Errors as a percentage of full scale range for each DOF for force balance 3